In-Situ Combustion Model

Keith H. Coats, Intercomp Resource Development and Engineering Inc.

Abstract

This paper describes a numerical model for simulating wet or dry, forward or reverse combustion in one, two, or three dimensions. The formulation is considerably more general than any reported to date. The model allows any number and identities of components. Any component may be distributed in any or all of the four phases (water, oil, gas, and solid or coke).

The formulation allows any number of chemical reactions. Any reaction may have any number of reactants, products, and stoichiometry, identified through input data. The energy balance accounts for heat loss and conduction, conversion, and radiation within the reservoir.

The model uses no assumptions regarding degree of oxygen consumption. The oxygen concentration is calculated throughout the reservoir in accordance with the calculated fluid flow pattern and reaction kinetics. The model, therefore, simulates the effects of oxygen bypassing caused by kinetic-limited combustion or conformance factors.

We believe the implicit model formulation results in maximum efficiency (lowest computing cost), and required computing times are reported in the paper.

The paper includes comparisons of model results with reported laboratory adiabatic-tube test results. In addition, the paper includes example field-scale cases, with a sensitivity study showing effects on oil recovery of uncertainties in rock/fluid properties.

Introduction

Recent papers by Ali,[1] Crookston *et al.*,[2] and Youngren[3] provide a comprehensive review of earlier work in numerical modeling of the in-situ combustion process.

0197-7520/80/0012-8394$00.25

The trend in this modeling has been toward more rigorous treatment of the fluid flow and interphase mass transfer; inclusion of more components, more comprehensive reaction kinetics, and stoichiometry; and more implicit treatment of the finite difference model equations.

The purpose of this work was to extend the generality of previous models while preserving or reducing the associated computing-time requirement. The most comprehensive or sophisticated combustion models described to date appear to be those of Crookston *et al.* and Youngren. Therefore, we compare our model formulation and results here with those models.

A common objective of different investigators' efforts in modeling in-situ combustion is development of more efficient formulations and methods of solution. This is especially important in the combustion case because of the large number of components and equations involved. For a given number of components and reactions, computing time per grid block per time step will increase rapidly as the formulation is rendered more implicit. However, increasing implicitness tends to allow larger time steps, which in turn reduces overall computing expense. To pursue the above objective, then, authors should present as completely as possible the details of their formulations and the associated computing-time requirements.

The thermal model described here simulates wet or dry, forward or reverse combustion in one, two, or three dimensions. The formulation allows any number and identities of components and any number of chemical reactions, with reactants, products, and stoichiometry specified through input data. The transient, three-phase flow is represented by Darcy's law, incorporating temperature-dependent relative permeabilities plus gravity,

viscous, and capillary forces. Vaporization/condensation phenomena are handled with allowance for any component to be distributed in any or all of the four phases. The fourth (solid or coke) phase is immobile and in part provides capability for treating in-situ coal gasification problems. Oxygen and fuel consumption are calculated in accordance with the specified reaction kinetics and calculated fluid flow patterns.

The following sections describe the model formulation both in general terms and in greater detail, with equations given. Several laboratory and field-scale applications are presented together with a set of sensitivity runs indicating the relative importance of different types of input data. The laboratory-scale model results are compared with the associated observed or experimental behavior.

While the model formulation was developed to simulate the in-situ combustion case, it applies also to hot-water or steamflooding and geothermal problems. Although certain features were introduced in the formulation with in-situ coal gasification in mind, no applications to that type of problem have been attempted to date.

General Comparative Model Description

Crookston *et al.*[2] describe a combustion model using the components oxygen, inert (noncondensable) gas, light hydrocarbon, heavy hydrocarbon, water, and coke. Their model accounts for the four chemical reactions representing oxidation of heavy oil, light oil, and coke and cracking of heavy oil. They treat three-phase fluid flow in one or two dimensions within the reservoir and use a two-dimensional heat conduction calculation for heat flow in the overburden. The additional variable introduced by the coke mass balance in their formulation is n_c lbm mol coke/cu ft of formation, and this mass is assumed to occupy negligible volume – i.e., $S_w + S_o + S_g = 1.0$ in their formulation. Crookston *et al.* use the mole-fraction constraints for oil and gas phases as primary equations and, thus, solve simultaneously a total of nine primary equations (six mass balances, one energy balance, and two mole-fraction constraints) using Gaussian elimination. They use a mixture of implicit and explicit treatment for coefficients in interblock transmissibilities and reaction terms.

Youngren[3] describes a three-dimensional combustion model that treats the five components – water, oxygen, nonvolatile oil, and two arbitrary volatile components – which can distribute between the oil and gas phases. He neglects coke formation and oxidation and treats the single chemical reaction of heavy oil oxidation. Oxygen is assumed to be consumed instantly on contact with fuel; therefore, combustion rate equals oxygen flux. The model simulates three-phase flow, and a one-dimensional, overburden heat conduction calculation is used for heat loss. Like Crookston *et al.*, Youngren uses a mixture of implicit and explicit treatment but, unlike them, he solves only four primary equations simultaneously, using Gaussian elimination. He reduces his six primary equations (five mass balances and one energy balance) to four equations by expressing the transmissibilities of Components 4 and 5 explicitly in mole fractions. All transmissibilities are explicit in temperature. Both models simulate convective and conductive heat flow within the reservoir.

The thermal model formulation described here allows any number and identities of components and any number of chemical reactions. Each reaction may have any number of reactants and products, identified through input data. Reaction rates are functions of temperature and reactant concentrations raised to powers specified through input data.

Without recourse to different "versions," the formulation applies to single-component (water) geothermal problems plus two-, three-, and four-component (e.g., including inert gas and/or distillable hydrocarbons) steamflooding or hot-water flooding problems and N_C-component in-situ combustion problems.

If a solid (coke) is one of the components, the model accounts for four phases, with S_4 representing the solid-phase saturation. Thus, our saturation constraint is $S_w + S_o + S_g + S_4 = 1.0$. Our experience indicates that coke (fuel) deposition can yield S_4 values in the 0.04 to 0.08 range. This may reduce formation permeability, and the formulation allows permeability to vary with the S_4 value.

The model uses no assumptions regarding degree of oxygen consumption. The oxygen concentration is calculated throughout the reservoir in accordance with the calculated fluid flow pattern and reaction kinetics. Youngren's assumption that combustion rate equals oxygen flux precludes application of his formulation to reverse combustion problems and problems where an oxidation reaction is kinetic rather than reactant limited. Also, as Youngren points out, his assumption prevents prediction of spontaneous ignition and his neglect of cracking or coke prevents prediction of fuel laydown.

In defense of Youngren's assumption regarding oxygen consumption, we must agree that most combustion problems probably are reactant limited. More important, however, we feel the assumption is simply unnecessary. That is, the assumption limits the applicability of a combustion model but yields little, if any, benefit in reduction of required arithmetic or computing time.

Unlike both models just discussed, the model presented here is completely implicit. Our experience in steamflood modeling[4-6] has led us to the belief that total computing expense for thermal-model runs decreases with increasing degrees of implicitness.

The model described here is a set of mass- and energy-balance equations and constraint equations written for each of a number of grid blocks representing a reservoir. The equations are written in finite difference form and include an energy balance and one mass balance for each of N_C components. The constraint equations express the requirements that fluid saturations must sum to unity and the mole fractions of components in each phase must sum to unity. Components are pure or pseudocompounds such as oxygen, nitrogen, carbon dioxide, water,

"heavy oil component," "light oil component," and solid component (coal or coke).

For maximum efficiency, these equations must be divided into groups: (1) $N_C + 1$ "primary" or "flow" equations (the energy balance and N_C-component mass balances) and (2) $N_P + 1$ constraints equations (one saturation constraint and N_P mole-fraction constraints). N_P is the number of phases, three or four. Constraint equations are used to eliminate $N_P + 1$ of the total $N_C + N_P + 2$ unknowns present in the $N_C + 1$ primary equations. The result is a set of $N_C + 1$ primary equations in $N_C + 1$ unknowns, which is solved by the reduced bandwidth direct solution technique described by Price and Coats.[7]

A major fraction of total model computing time may be expended in this direct solution of the primary equations. The arithmetic required in this direct solution is proportional to the cube of the number of primary equations solved.[6] Thus, it is important to minimize this number by using all constraint equations to eliminate unknowns. Crookston *et al.* retain two mole-fraction constraints in their set of primary equations and, thus, use direct solution (Gaussian elimination) to solve a set of nine primary equations for problems involving N_C = six components. The formulation described here actually results in direct solution of a set of only six primary equations for the case of six components if one of the components is coke. This set of N_C rather than $N_C + 1$ primary equations is attained through use of the coke mass balance as a constraint equation, which in turn is possible because the coke is immobile. This is discussed in detail in the mathematical model description.

This discussion suggests that Youngren's approach of solving only four primary equations, regardless of the number of components, may result in less computing expense than the implicit formulation described here. His formulation certainly will, or should, require less arithmetic on a grid-block/time-step basis. However, we must consider the penalty associated with the method by which he attains a primary set of only four equations. The method involves use of explicit mole fractions $x_4, x_5, \ldots, x_{N_C}$ in the transmissibilities of the Component 4, 5 ..., N_C mass balances. A stability analysis of multicomponent, single-phase flow shows that this explicit treatment give a time-step limitation,

$$\Delta t < S_g \, \Delta x / v_{gx} ,$$

where Δx is the grid block dimension in feet and v_{gx} is gas-phase interstitial velocity in feet per day. We can substitute $\Delta y / v_{gy}$ or $\Delta z / v_{gz}$ for $\Delta x / v_{gx}$. In steamflood or combustion problems, v_g can reach locally large values (e.g., 10 to 20 ft/D or more), even with low S_g values. We feel this stability limit on time-step size will cause in many cases a sufficiently increased number of required time steps to more than offset the reduced arithmetic *per time step*. However, for some sufficiently large number of components, the implicit formulation requiring direct solution of $N_C + 1$ primary equations will require more total computing time than Youngren's formulation.

The model described here simulates wet or dry forward combustion and reverse combustion in one, two, or three dimensions. The model equations describe mass transport by Darcy flow, incorporating gravity, viscous, and capillary forces. The heat transport includes mechanisms of convection, radiation, and conduction within the reservoir and conductive heat loss to the overburden and underlying strata.

The model allows any component to be distributed in any or all of four phases (water, oil, gas, and solid) as dictated by read-in pressure- and temperature-dependent component K-values. Each phase density is a function of its composition, pressure, and temperature. Gas-phase supercompressibility factor s is obtained from the Redlich-Kwong equation of state.[8]

The generality in respect to component distribution among phases allows study of the effect of CO_2 solution in oil with attendant reduction in oil viscosity. Also, CO_2 or any component may be assigned some solubility in the liquid water phase. An interesting potential of this generality is examination of emulsion effects. Specifying solubility of water in the oil phase or of oil components in the water phase and adjusting input-component viscosity data can yield emulsion-type viscosities for the oil or water phase.

The formulation achieves this generality of component distribution by assigning a user-specified "master" phase to each component with a resulting single set of master mole fractions $\{X_i\}$. User-specified pressure- and temperature-dependent K-values then give the mole fraction of each component i in phase j as $x_{ij} = K_{vij} X_i$. This treatment simplifies model description, coding logic, and variable substitution logic since it avoids the need to deal with four sets of phase mole fractions.

The inclusion of a fourth (solid) phase in the formulation represents a step toward the capability to simulate in-situ coal gasification. In this case, the initialized Phase 4 saturation would be large (e.g., 0.8), representing the coal itself. The formulation treats relative permeabilities as functions of normalized saturations (e.g., $S_w = S_w / 1 - S_4$) to represent more reasonably the case where S_4 is large and highly variable. The model reaction kinetics require alteration in form for the gasification problem since coal gasification reactions generally reach an equilibrium between reactants and products.

Mathematical Description of Model

The model consists of N equations where $N = N_C + N_P + 2$ and N_P denotes the number of phases present. $N_P = 4$ if solid coke is present in addition to the water, oil, and gas phases. $N_P = 3$ if no solid phase exists or appears. The model equations are

N_C	Component mass balance equations
1	Energy balance equation
1	Saturation constraint
N_P	Mole fraction constraints
$N_C + N_P + 2$	Total equations .

The saturation constraint expresses the fact that the N_P phase saturation must sum to unity. The N_P mole-fraction constraints express the requirement that the sum of all components' mole fractions in each phase must sum to unity.

We refer to phases by the index or subscript J, with $J = 1$ for liquid water, $J = 2$ for oil, $J = 3$ for gas, and $J = 4$ for the solid phase. Components are denoted by index or subscript I, with

I	Component
2	Water
2	Heavy-oil component
3	Gaseous component
4	Coke if a solid component is present
4	Gaseous or oil component if solid component is not present
$5 - N_C$	Gaseous or oil components.

The N model equations for each grid block follow.

Component Mass Balances $I = 1, 2, \ldots, N_C$

$$\frac{V}{\Delta t}\bar{\delta}\left(\phi \sum_{J=1}^{N_P} \rho_J S_J x_{IJ}\right) = \sum_{J=1}^{3} \Delta\, \tau \rho_J x_{IJ} \frac{k_{rJ}}{\mu_J} \cdot \left(\Delta p + \Delta P_{cj} - \gamma_J \Delta Z\right) + \sum_{r=1}^{N_R} q_{Ir} - q_I \,. \quad \ldots\ldots (1)$$

Energy Balance

$$\frac{V}{\Delta t}\bar{\delta}\left[\phi \sum_{J=1}^{N_P} \rho_J S_J U_J + (1-\phi) M_f (T - T_i)\right] = \sum_{J=1}^{3} \Delta\left[\tau \rho_J \frac{k_{rJ}}{\mu_J} H_J (\Delta p + \Delta P_{cJ} - \gamma_J \Delta Z)\right] + \Delta(\tau_c \Delta T) + \Delta(\tau_R \Delta T^4) + \sum_{r=1}^{N_R} H_r - \dot{Q}_H - \dot{Q}_{HL} \,. \quad \ldots\ldots (2)$$

Saturation Constraint

$$\sum_{J=1}^{N_P} \bar{\delta} S_J = 0 \,. \quad \ldots\ldots (3)$$

Mole-Fraction Constraints $J = 1, 2, \ldots, N_P$

$$\sum_{I=1}^{N_C} x_{IJ} = 1.0 \,. \quad \ldots\ldots (4)$$

We have suppressed the grid-block subscript indices i, j, and k on all terms in these equations.

The mole fraction of component I in phase J is calculated as

$$x_{IJ} = K_{vIJ} X_I \,, \quad \ldots\ldots (5)$$

where K_{vIJ} are equilibrium K-values and X_I is the mole fraction of component I in component I's primary or "master" phase. Thus, if phase ℓ is phase I's primary phase, then $K_{vI\ell} \equiv 1.0$. If component I is not present ("soluble") in phase J, then $K_{vIJ} \equiv 0$.

The N unknowns corresponding to the Eqs. 1 through 4 are δS_1, δS_2, ..., δS_{N_P}, δX_1, δX_2, ..., δX_{N_C}, δp, δT. All terms in Eqs. 1 through 4 can be expressed in terms of these unknowns.

Treatment of Accumulation (Left-Side) Terms

The left side of the component mass balance can be expressed as

$$\frac{V}{\Delta t}\bar{\delta}\left(\sum_{J=1}^{N_P} \rho_J S_J K_{vIJ} X_I\right) = \frac{V}{\Delta t}\left[\left(\phi \sum_{J=1}^{N_P} \rho_J S_J K_{vIJ} X_I\right)^{\ell} - \left(\phi \sum_{J=1}^{N_P} \rho_J S_J K_{vIJ} X_I\right)_n\right] + \frac{V}{\Delta t} \sum_{m=1}^{N_P} \left[\frac{\partial}{\partial P_m} \cdot \left(\sum_{J=1}^{N_P} \rho_J S_J K_{vIJ} X_I\right)\right]^{\ell} \delta P_m \,, \quad \ldots\ldots (6)$$

where superscript ℓ denotes the latest iterate value, subscript n denotes the time level n value, and N is the number of total unknowns. The N unknowns $\{\delta P_j\}$ are changes over the iteration

$$\begin{aligned} \delta P_1 &\equiv \delta S_1 \\ \delta P_2 &\equiv \delta S_2 \\ &\vdots \\ \delta P_{N_P} &\equiv \delta S_{N_P} \\ \delta P_{N_P+1} &\equiv \delta X_1 \\ \delta P_{N_P+2} &\equiv \delta X_2 \\ &\vdots \\ \delta P_{N_P+N_C} &\equiv \delta X_{N_C} \\ \delta P_{N_P+N_C+1} &\equiv \delta p \end{aligned}$$

and

$$\delta P_{N_P+N_C+2} \equiv \delta T \,. \quad \ldots\ldots (7)$$

Differentiation of a product of terms is performed by the normal chain rule,

$$\frac{\partial}{\partial P}(abc)^{\ell} \equiv (ab)^{\ell}\frac{\partial c}{\partial P} + (ac)^{\ell}\frac{\partial b}{\partial P} + (bc)^{\ell}\frac{\partial a}{\partial P} \,.$$

The derivatives in the last term of Eq. 6 are evaluated at the latest iterate (ℓ) values of all unknowns. The energy-balance accumulation term is expanded in the same manner as Eq. 6.

Interblock Fluid-Flow (Right-Side) Terms

The interblock flow terms are treated implicitly. The flow term for phase J in the component mass balance is expanded as

$$\left[\tau \rho_j K_{vIJ} X_I \frac{k_{rJ}}{\mu_J}\left(\Delta p + \Delta P_{cJ} - \gamma_J \Delta Z\right)\right] \cong \left[\tau \rho_J K_{vIJ} X_I \frac{k_{rJ}}{\mu_J}\left(\Delta p + \Delta P_{cJ} - \gamma_J \Delta Z\right)\right]^{\ell}$$

$$+\sum_{m=1}^{N}\frac{\partial}{\partial P_m}\left[\tau\rho_J K_{vIJ}X_I\frac{k_{rJ}}{\mu_J}\left(\Delta p+\Delta P_{cJ}-\gamma_J\Delta Z\right)\right]^{\ell}\delta P_m \quad \ldots\ldots\ldots\ldots\ldots\ldots (8)$$

If Eq. 8 denotes interblock flow between two adjacent grid blocks, denoted as Block 1 and Block 2, then the weighting of terms is upstream for $(\rho/\mu)_J$, k_{rJ}, x_{IJ}, and

$$\gamma_J = \omega\gamma^{\ell}_{J1}+(1-\omega)\gamma^{\ell}_{J2} \quad \ldots\ldots\ldots\ldots\ldots\ldots (9)$$

where ω is $(V\phi)_1/[(V\phi)_1+(V\phi)_2]$.

Interblock Heat-Flow Terms

Interblock heat flow between Grid Blocks 1 and 2 includes transport by convection (enthalpy flow associated with mass flow), conduction, and radiation. The flow due to conduction and radiation is

$$q = \frac{\lambda A}{L}\left(T_1-T_2\right)+\frac{\alpha_3\lambda_i A}{L}\left(T_1^4-T_2^4\right)\text{Btu/D}, \quad \ldots\ldots\ldots\ldots\ldots\ldots (10)$$

where A is the cross-sectional area normal to flow, L is the distance between grid-block centers, and α_3 is read as input data. We have generally used $\alpha_3 = 0$. In accordance with the implicit representations throughout the model, this heat flow is calculated as

$$q = q^{\ell}+\sum_{m=1}^{N}\frac{\partial}{\partial P_m}\left[\frac{\lambda A}{L}\left(T_1-T_2\right)+\frac{\alpha_3\lambda_i A}{L}\left(T_1^4-T_2^4\right)\right]^{\ell}\delta P_m \quad \ldots\ldots\ldots\ldots (11)$$

The interblock weighting of enthalpy in the energy-balance interblock flow terms is

$$H_J = \theta H_{J\text{up}}+(1-\theta)H_{J\text{down}}, \quad \ldots\ldots\ldots\ldots (12)$$

where $0.5 \le \theta \le 1.0$ and "up" and "down" denote upstream and downstream blocks for flow of phase J. We use $\theta = 0.5$ as a default value, with provision for the user to change the value through input data.

Treatment of Chemical Reaction Terms

The rate of the chemical reaction number r is

$$R_r = VA_r e^{-\frac{1.8E_r}{RT}}\cdot\prod_{j=1,N_{R,r}}\left(\phi\rho_{m_{jr}}S_{m_{jr},m_{jr}}\right)^{n_{j,r}}, \quad \ldots\ldots\ldots (13)$$

with units of moles per day for the first reactant. For gaseous reactants, the user may specify a partial pressure in place of concentration. For the cracking reaction, an additional multiplicative factor of $1-[S_4/(S_4)_{\max}]^n$ is used in Eq. 13. This factor was proposed by Crookston *et al.* as a means of limiting the coke (fuel) formation. If $(S_4)_{\max}$ is read as zero in input data, then this additional factor is not used.

For illustration we consider the specific reaction (r) of oxidation of a Heavy Oil Component 2. Oxygen is Component 6. The reaction stoichiometry is

$$s_{1r}\text{oil}_2+s_{2r}O_2 \rightarrow s_{3r}CO_2+s_{4r}H_2O \quad \ldots\ldots\ldots (14)$$

The stoichiometric coefficient of the first reactant, S_{1r}, is 1.0 by definition. The reaction rate in moles of first reactant per day for the grid block is

$$R_r\ \frac{\text{moles Component 2}}{\text{D}} = VA_r e^{-\frac{1.8E_r}{RT}}\left(\phi S_2\rho_2 x_{22}\right)^{n_{1r}}\cdot\left(\phi S_3\rho_3 x_{63}\right)^{n_{2r}}. \quad \ldots\ldots\ldots (15)$$

The heat of reaction is

$$H_r = R_r H_{r1}\text{Btu/D}. \quad \ldots\ldots\ldots (16)$$

The rates of appearance of energy and Components 2, 6, 3 (CO_2), and 1 (H_2O), which are required in Eqs. 1 and 2 are

$$q_{2r} = -R_r \text{ mol/D}$$
$$q_{6r} = -s_{2r}R_r$$
$$q_{3r} = s_{3r}R_r$$
$$q_{1r} = s_{4r}R_r$$

and

$$q_{N_C+1,r} = H_r, \quad \ldots\ldots\ldots (17)$$

where "component" $N_C + 1$ is energy.

The reaction rate is computed at the start of each iteration as

$$R_r = \left[VA_r e^{-\frac{1.8E_r}{RT}}\left(\phi S_2\rho_2 x_{22}\right)^{n_{1r}}\cdot\left(\phi S_3\rho_3 x_{63}\right)^{n_{2r}}\right]^{\ell}+VA_r\sum_{m=1}^{N}\frac{\partial}{\partial P_m}\cdot\left[e^{-\frac{1.8E_r}{RT}}\left(\phi S_2\rho_2 x_{22}\right)^{n_{1r}}\cdot\left(\phi S_3\rho_3 x_{63}\right)^{n_{2r}}\right]^{\ell}\delta P_m, \quad \ldots\ldots\ldots (18)$$

where the grid-block volume V and the reaction-rate constant A_r are constants. The user may specify partial pressure rather than concentration for a gaseous reactant so that px_{63} may replace $\phi S_3\rho_3 x_{63}$ in the preceding equations.

Temperature in the Arrhenius exponent is evaluated as $0.5\,(T_{n+1}+T_n)$ and oil saturation is evaluated as $0.5\,(S_{2n+1}+S_{2n})$ if all iterate values S_2^{ℓ} are positive and as S_{2n+1} if any iterate value S_2^{ℓ} is negative.

Treatment of Well Terms

We discuss the case of a production well on deliverability completed in three layers, denoted by $k = 1$, 2, and 3. Each layer is assigned a time-independent productivity index PI_k. The phase production rates from each layer are

$$q_{Jk} = \mathrm{PI}_k\left(\frac{k_{rJ}}{\mu_J}\right)_k (p_k - p_{wbk}) \quad \ldots\ldots\ldots (19)$$

where p_k is grid-block pressure and p_{wbk} is flowing bottomhole wellbore pressure opposite the center of grid block k. A flowing wellbore gradient is calculated for each layer as

$$\gamma_{wbk} = \sum_{J=1}^{3}\left(\frac{k_{rJ}}{\mu_J}\rho\gamma_J\right)_k \Big/ \sum_{J=1}^{3}\left(\frac{k_{rJ}}{\mu_J}\right)_k \rho, \quad \ldots\ldots\ldots (20)$$

which is a volumetric average gradient. The γ_{wbk} are calculated at the start of each time step and are used unchanged for succeeding iterations. The flowing wellbore pressure then is calculated as

$$p_{wbk} = p_{wbk-1} + \left(\gamma_{wbk-1}\alpha_{k-1} + \gamma_{wbk}\alpha_k\right)\left(Z_k - Z_{k-1}\right), \quad \ldots\ldots\ldots (21)$$

where Z_k is depth to the center of grid block k and p_{wbl} is a specified limiting bottomhole flowing pressure. The weight factors account for differing layer thicknesses, $\alpha_k = 0.5\Delta Z_k/(Z_k - Z_{k-1})$ and $\alpha_{k-1} = 1 - \alpha_k$, where ΔZ_k is the (vertically measured) thickness of layer k.

The production rate of component I from layer k is calculated as

$$q_{IK} = \mathrm{PI}_k\left[\sum_{j=1}^{3}\left(\frac{\rho}{\mu}k_r\right)_J K_{vIJ}X_I(p - p_{wb})\right]_k^{\ell} + \mathrm{PI}_k\sum_{m=1}^{N}\frac{\partial}{\partial P_m}\left[\sum_{J=1}^{3}\left(\frac{\rho}{\mu}k_r\right)_J K_{vIJ}X_I \cdot (p - p_{wb})\right]_k^{\ell}\delta P_m, \quad \ldots\ldots\ldots (22)$$

where p_{wbk} is held constant in the differentiation.

The enthalpy production rate in Eq. 2 from grid block k is

$$\dot{Q}_{HK} = \mathrm{PI}_k\left[\sum_{J=1}^{3}\left(\frac{\rho}{\mu}k_r\right)_J H_J(p - p_{wb})\right]_k^{\ell} + \mathrm{PI}_k\left[\sum_{m=1}^{N}\frac{\partial}{\partial P_m}\sum_{J=1}^{3}\left(\frac{\rho}{\mu}k_r\right)_J \cdot (p - p_{wb})\right]_k^{\ell}\delta P_m . \quad \ldots\ldots\ldots (23)$$

Heat-Loss Treatment

The implicit calculation of heat loss is calculated as described in detail in Ref. 4. The $\dot{Q}_{HL}$ term in Eq. 2 is replaced by a term of type $\alpha_1 - \alpha_2\delta T$.

Functional Dependency

The fluid and rock properties are dependent on the system variables:

ρ_J, μ_J, γ_J	$f(p,T,X)$
k_{rJ}	$f(S,T)$
λ	$f(S_g)$
k	$f(S_4)$
M_f	$f(T)$
K_{vIJ}	$f(p,T)$
H,U	$f(p,T)$
ϕ	$f(p)$

Here, X denotes dependence on $\{X_i\}$ and S denotes dependence on $\{S_J\}$. The Appendix describes the PVT treatment of rock and fluid properties.

Treatment of Constraint Equations

The saturation constraint (Eq. 3) is expressed simply at each iteration as

$$\sum_{J=1}^{N_P}\delta S_J = 0 . \quad \ldots\ldots\ldots (24)$$

In the mole-fraction constraints (Eq. 4), we have

$$x_{IJ} = (K_{vIJ}X_I)^{\ell} + \sum_{m=1}^{N}\frac{\partial}{\partial P_m}(K_{vij}X_I)^{\ell}\delta P_m, \quad \ldots\ldots\ldots (25)$$

so that the constraints (Eq. 4) become

$$\sum_{I=1}^{N_C}\left[\sum_{m=1}^{N}\frac{\partial}{\partial P_m}(K_{vIJ}X_I)\,\delta P_m\right] = 1 - \left(\sum_{I=1}^{N_c}K_{vIJ}X_I\right)^{\ell}. \quad \ldots\ldots\ldots (26)$$

Consolidation of $N_C + 2$ Model Equations

The preceding sections describe the expansion of all terms in Eqs. 1 through 4 in linearized expansions consisting of coefficients times iterate changes δP_m, $m = 1, 2, \ldots, N$, where $N = N_C + N_P + 2$. Only the first $N_C + 1$ of these N equations possess right-side flow terms that introduce unknowns $\{\delta P_m\}$ of neighboring grid blocks. These $N_C + 1$ equations are designated "primary" equations. The remaining $N_P + 1$ equations are constraint equations, and they are used to eliminate $N_P + 1$ unknowns from the primary equations. This elimination is possible because the constraint equations for a given grid block involve only unknowns $\{\delta P_m\}$ of that grid block.

For that moment, we neglect the interblock flow terms in Eqs. 1 through 4 and consider the accumulation and all other terms. After the expansion described previously, the N equations can be written as

$$\sum_{J=1}^{N}C_{ij}\delta P_J = b_i;\ i = 1, 2, \ldots, N, \quad \ldots\ldots (27)$$

where we locally use i as the equation number and j as the column or unknown index. The equations for $i = 1, 2, \ldots, N_C$ are component mass balances. The equation for $i = N_C + 1$ is the energy balance. The equation for $i = N_C + 2$ is the saturation constraint. The equations for $i = N_C + 3, N_C + 4, \ldots, N$ are the mole-fraction constraints. The coefficients C_{ij} and b_i terms are evaluated at latest iterate (ℓ) values of the unknowns $\{P_j\}$.

The last N_P of these equations are mole-fraction constraints and coefficients C_{ij} are all zero for $j = 1$,

2, ..., N_P, since unknowns δP_1 through δP_{N_P} are δS_1 through δS_{N_P} and the mole-fraction constraints do not involve fluid saturations. Coefficients C_{ij} for $j = N_P + 1, N_P + 2, \ldots, N$ are generally nonzero. We diagonalize this submatrix of N_P equations by Gaussian elimination so that the last N_P (mole-fraction constraint) equation's matrix is reduced to

$$
\begin{array}{rccccc}
j = & N_P+1 & N_P+2 & \ldots\ 2N_P & 2N_P+1 \\
i=N_C+3 & 1 & 0 & 0 & \checkmark \\
i=N_C+4 & 0 & 1 & 0 & \checkmark \\
\vdots & \vdots & & & \\
i=N_C+N_P+2 & 0 & 0 & 1 & \checkmark
\end{array}
$$

$$
\begin{array}{rccc}
j = & \ldots N & & \\
i=N_C+3 & \checkmark & \delta P_{N_P+1} & \checkmark \\
i=N_C+4 & \checkmark & \delta P_{N_P+2} = & \checkmark \\
\vdots & & \vdots & \vdots \\
i=N_C+N_P+2 & \checkmark & \delta P_N & \checkmark\ ,
\end{array}
\quad \ldots\ldots\ldots\ldots\ldots\ldots\ldots\ldots\ldots\ldots (28)
$$

where the check marks indicate nonzero coefficients. These diagonalized N_P mole-fraction constraints are used to eliminate Columns (unknowns) $j = N_P + 1$, $N_P + 2$, ..., $2N_P$ in the first $N_C + 1$ equations of the equation set (Eq. 27).

The saturation constraint (Eq. 24) then is used to eliminate Column N_P from the first $N_C + 1$ equations of Eq. 27. This now leaves $N_C + 1$ equations (which involve right-side interblock flow terms) and $N_C + 1$ unknowns. We started with $N_C + N_P + 2$ unknowns, but we eliminated N_P unknowns (mole fractions) using the N_P mole-fraction constraints and eliminated one unknown (saturation) using the saturation constraint.

The coefficients in the reduced mole-fraction-constraint matrix (Eq. 28) are saved or stored for two reasons: (1) they are needed to eliminate the mentioned columns from the expansions on the interblock flow terms and (2) they are needed after solution of the $N_C + 1$ equations to compute the eliminated unknowns. Similarly, δS_{N_P}, which was eliminated, is calculated after solution of the $N_C + 1$ equations.

The $N_C + 1$ primary equations can be written in matrix form as

$$\underline{C}\underline{P} = \underline{R} + \Delta(\tau \Delta \underline{P}) \ , \ldots\ldots\ldots\ldots\ldots\ldots (29)$$

where C and τ are $(N_C + 1) \times (N_C + 1)$ matrices and $\underline{R}$ and $\underline{P}$ are $N_C + 1$ column vectors. These equations are solved by the reduced bandwidth direct solution technique.[7] Eqs. 28 and the saturation constraint then are used to calculate the eliminated unknowns. The cumulative changes over the time step then are augmented as

$$\bar{\delta} P_j^{\ell+1} = \bar{\delta} P_j^{\ell} + \delta P_j \ , \ldots\ldots\ldots\ldots\ldots\ldots\ldots (30)$$

where a damping factor may be applied to δP_j in Eq. 30 if one or more of the iterate changes δP_j are excessive.

C, τ, and R in Eq. 29 are re-evaluated using the latest iterate values of $\{P_j\}$, and Eq. 29 is solved again. These iterations are terminated when all the following are satisfied.

$$\max_{j=1,N_P} | \delta S_j | \leq \text{TOLS } (0.01) \ ,$$

$$\max_{i=1,N_C} | \delta X_i | \leq \text{TOLX } (0.01) \ ,$$

$$\max | \delta p | \leq \text{TOLP } (1.0) \ ,$$

and

$$\max | \delta T | \leq \text{TOLT } (1.0) \ , \quad \ldots\ldots (31)$$

where "max" denotes maximum over all grid blocks and default closure tolerance values are given in parentheses.

Variable Substitution

The $N_P + 1$ constraint equations are used to eliminate $N_P + 1$ unknowns, resulting in a set of $N_C + 1$ (mass- and energy-balance) primary equations in $N_C + 1$ remaining unknowns. In the general case, where all four saturations are nonzero, the eliminated unknowns are δX_1, δX_2, δX_3, δX_4, and δS_4, leaving δS_1, δS_2, δS_3, δX_5, ..., δX_{N_C}, δp, and δT as the $N_C + 1$ "primary" unknowns.

If any saturation S_j is zero for some iteration, then no mole-fraction constraint exists for phase j and we ostensibly have one less unknown (δS_j) and one less equation. In actuality, however, we still have $N_C + 1$ primary equations in $N_C + 1$ unknowns, with one less *constraint* equation counterbalanced by one less *eliminated* unknown. That is, δX_j is not eliminated and δX_j takes the place of δS_j in the $N_C + 1$ unknowns. The δS_j is known a priori as $-S_{j,n}$. An example of this substitution of δX_j for δS_j is the onset of the superheated water state, where S_1 becomes zero but δX_1 still requires calculation since the gas phase will contain a water mole fraction of $K_{v13} X_1$.

One important exception to this description of $N_C + 1$ primary equations in $N_C + 1$ primary variables is introduced by the immobility of coke. If coke is one of the N_C components, we can reduce the system of N equations to only N_C rather than $N_C + 1$ primary equations. This is important because the computing time required for simultaneous, direct solution of the primary equations (1) is proportional to the cube of the number of primary equations and (2) can constitute 80% or more of total computing time.[6]

If coke is one component, then the primary equations (involving right-side flow terms) are the energy equation and the $N_C - 1$ mass balances for the $N_C - 1$ mobile components. The coke mass-balance equation becomes a constraint equation. The

mole-fraction constraint for Solid Phase 4 is used to eliminate δX_4 [mole fraction of Component 4 (coke) in the solid phase] from all N equations and then the resulting coke balance is used to eliminate δS_4 from the primary equations. The saturation constraint is used to eliminate $\delta S_{j\max}$ from the primary equations, where $j$max is less than 4 and is the largest value of j for which S_j^f is positive.

Miscellaneous

Model initialization requires specification of initial-phase mole fractions, temperature, gas/oil and/or water/oil contacts, and pressure at a specified subsea datum. The model initializes pressure either by capillary-gravitational equilibrium or by setting pressure to a constant, at the user's option. If a gas phase is initially present, the model automatically will recalculate the mole fraction of a specified "swing" component to attain a sum to unity of gas-phase mole fractions. This swing component generally is specified as N_2 or a N_2 + CO_x pseudocomponent. The reason for this internal resetting of a gas-phase mole fraction is the difficulty in calculating by hand the initial mole fractions of distributed components so that the gas-phase mole-fraction sum will exactly equal unity.

The material balance at each time step for each component is calculated as

1 + mass in place − (initial mass in place

+ cumulative injection − cumulative production

+ net production by reactions)

÷ max (cumulative injection, cumulative production)

+ max (reaction production, reaction consumption) .

The energy balance is calculated in the same manner with "energy" substituted for "mass." Values of 1.0000 for these balances simply indicate that the finite difference equations are solved accurately.

Automatic time-step control is used with time-step size controlled by the previous step size and the previous step changes (maximum over grid) in saturation pressure, temperature, and mole fraction.

Applications

In all the model runs described below $(S_4)_{\max}$ and heats of vaporization for volatile oil components are zero. Our experience indicates a negligible effect of heat of vaporization. No temperature dependence of relative permeability or capillary pressure is present in any of the problems. Units missing from problem data listed in tables are given in the Nomenclature. Partial pressure is used in lieu of concentration for oxygen in all oxidation reactions.

While the ASTM form for oil-component viscosity (Eq. A-20) currently is programmed in the model, the model runs described here used the form

$$\mu_{IJ} = a\, e^{b/T} ,$$

for liquid phases J = 1 or 2, which is the representation used by Crookston *et al.*[2]

All model runs were performed using midpoint convective weighting (θ = 0.5 in Eq. 12).

Smith and Perkins Experiment

Smith and Perkins[9] conducted wet, forward combustion experiments in a vertical, adiabatic combustion tube. They injected a constant-ratio air/water stream into a 700-md, 120°F vertical tube 5.75 ft long after preheating the top to 600°F. They reported (1) measured temperature profiles at 2, 4, and 6 hours, (2) percent unused oxygen in the produced gas phase vs. cumulative air injection, and (3) amount of oil burned. They also described a numerical model and compared their calculated with their experimental results.

Smith and Perkins reported two experiments – a low-pressure test using Crude A and a high-pressure test using Crude B. Results discussed here are for the 815-psia low-pressure run. Crude A is very light with API gravity and viscosity of 36° and 2.8 cp, respectively. They presented a temperature profile at time zero corresponding to the heating at the tube top price prior to air injection. They further stated that the air/water injection-stream temperature varied from an initially high value (due to preheating of the upper tube apparatus) to a later value of (presumably) 120°F. We simply initialized the first 20% of tube length to 500°F and the remaining 80% to 120°F and injected at a constant 120°F.

Smith and Perkins reported an initial period of air injection with no water. This air injection was continued until they noticed vigorous combustion and no oxygen in the effluent gas. They did not report the time period of this dry air injection. We used 28.8 minutes. The subsequent water/air ratio was constant at 0.18 lbm/scf.

Smith and Perkins stated their insulation was unusually permeable and heat convected outside the tube from the burning front upward to the trailing edge. They accounted for this external convection in their numerical model and reported better trailing-edge agreement than we obtained.

We changed Smith and Perkins' six-component oil analysis to three components and treated the six-component system given in Table 1. We calculated K-values for each of the original six oil components from $\ln p_v = A - B/T$, with A and B determined from boiling-point and critical data given in Ref. 10. Viscosity coefficients were obtained for the six components from the same reference. K-value and viscosity parameters for the three pseudo oil components then were calculated by simple mole-fraction weighted averages.

Smith and Perkins represented the oil oxidation by

$$\frac{dO_2}{dT} = A_o p_{O_2}\, e^{-\frac{B}{T} - Cf} \quad \ldots\ldots\ldots\ldots\ldots\ldots (32)$$

where p_{O_2} is partial of oxygen; A_o, B, and C were determined from experimental data; and f is the fraction of oil oxidized. We used a reaction proportional to

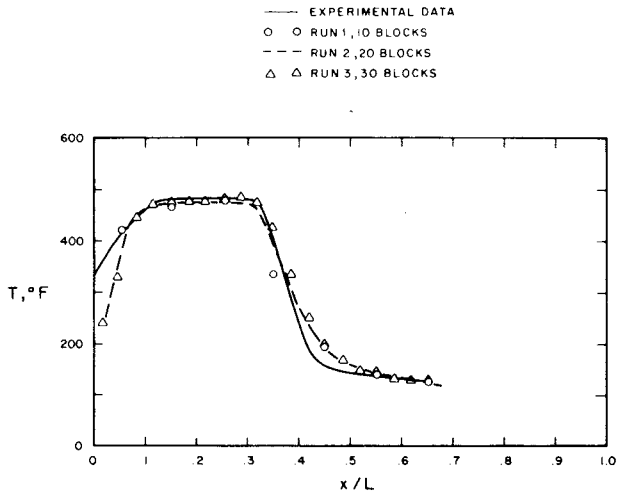

Fig. 1 – Calculated and observed 2-hour temperature profile – Smith-Perkins experiment.

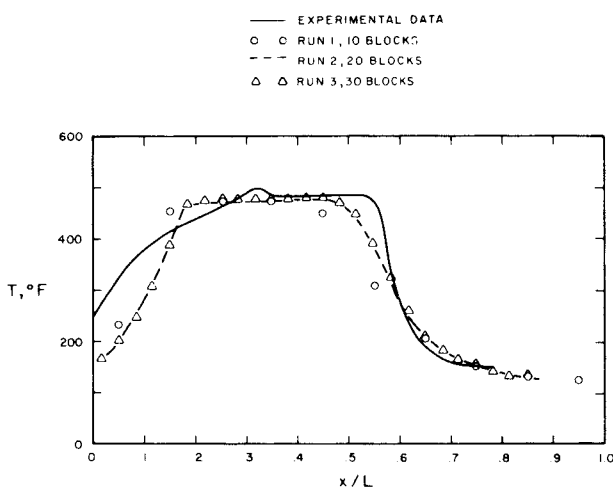

Fig. 2 – Calculated and observed 4-hour temperature profile – Smith-Perkins experiment.

TABLE 1 – DATA FOR SMITH-PERKINS LABORATORY TEST

Vertical tube length, ft	5.75
Tube cross-sectional area, sq ft	0.0834
Permeability, md	700
Porosity	0.25
Rock heat capacity, Btu/cu ft rock-°F	$34\,[1 + 0.00055(T - T_i)]$
Thermal conductivity, Btu/ft-D-°F	3.0
Initial temperature, °F in first 20% of tube length	500
°F in last 80% of tube length	120
P_o, psia	815
Initial water, oil, gas saturations	0.3, 0.4, 0.3
Initial mole fractions, $X_1 = 1.0, X_2 = 0.2063, X_3 = 0.71,$ $X_4 = 0.084, X_5 = 0.7097, X_6 = 0.29$	
Number grid blocks (three one-dimensional runs)	10, 20, and 30
Number of components	6
Number of reactions	3

Viscosity Data

$\mu_{22} = 0.02772\, e^{3,363/T}$
$\mu_{23} = 0.08$
$\mu_{33} = 0.0002127\, T^{0.702}$
$\mu_{42} = 0.01\, e^{4,908/T}$
$\mu_{52} = 0.0358\, e^{2,135/T}$
$\mu_{53} = 0.03$
$\mu_{63} = 0.0002196\, T^{0.721}$

Reaction Data

C_i denotes Component i

Component i	Molecular	p_c	T_c(°R)	c_i	β_i	C_{PI}(Btu/lbm)
1. H_2	18	3,206.2	1,165.4			
2. C_{20}	282.6	162	1,381	10^{-5}	0.00038	0.6
3. $N_2 - CO_x$	32	750	350			0.226
4. $C_{32} + C_{47}$	508.9	50.7	1,598	10^{-5}	0.00038	0.6
5. $C_6 + C_8 + C_{12}$	131.4	336.6	1,067	10^{-5}	0.00038	0.6
6. O_2	32	730	277.9			0.24

$v^o_{22} = 0.01767$ cu ft/lbm
$v^o_{42} = 0.01635$ cu ft/lbm
$v^o_{52} = 0.02228$ cu ft/lbm

Stock-tank densities for Components 2, 4, and 5: 56.6, 61.15, and 44.9 lbm/cu ft

Reaction r	Stoichiometry
1	$C_2 + 25.08\, C_6 \rightarrow 16.5\, C_1 + 20.8\, C_3$
2	$C_4 + 45.17\, C_6 \rightarrow 29.71\, C_1 + 37.46\, C_3$
3	$C_3 + 11.66\, C_6 \rightarrow 7.67\, C_1 + 9.67\, C_3$

	Rate Constant $A_r \times 10^{-10}$	Activation Energy E_r	Heat of Reaction H_{r1} (Btu/lbm oil)
1	0.28164	18,214	16,000
2	3.4054	18,214	16,000
3	0.4035	18,214	16,000

Relative Permeability and Capillary Pressure Data

Capillary pressure = 0
$S_{wi} = S_{wir} = S_{orw} = 0.25$
$S_{org} = 0.9$
$k_{rwro} = 0.5$
$k_{roiw} = 1.0$
$k_{rgro} = 1.0$
$n_w = n_{ow} = n_{og} = n_g = 2.0$

K-Value Data

$K_{v23} = (3.11 \times 10^6/p)\, e^{-13,620/T}$
$K_{v43} = 0$
$K_{v53} = (7.668 \times 10^5/p)\, e^{-8,331/T}$

Injection/Production Data

Air injection mode, scf/D	108.1
Water/air ratio for first 28.5 minutes	0
lbm/scf air after 28.8 minutes	0.18
Production at tube outlet at constant pressure, psia	815

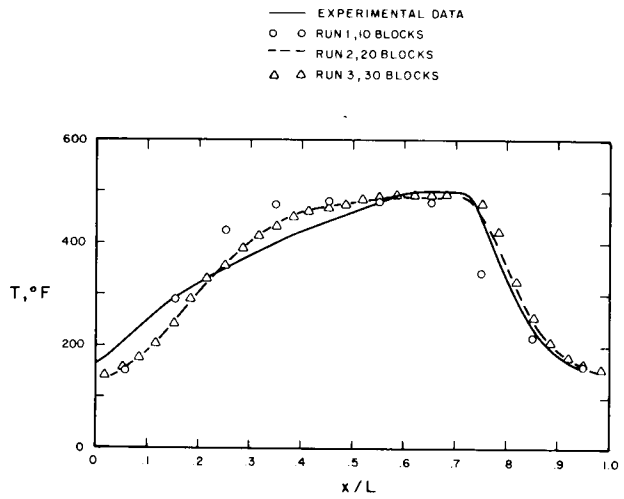

Fig. 3 – Calculated and observed 6-hour temperature profile – Smith-Perkins experiment.

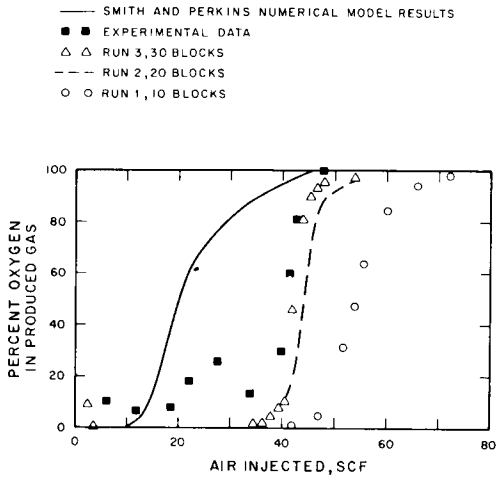

Fig. 4 – Calculated and observed oxygen breakout times – Smith-Perkins experiment.

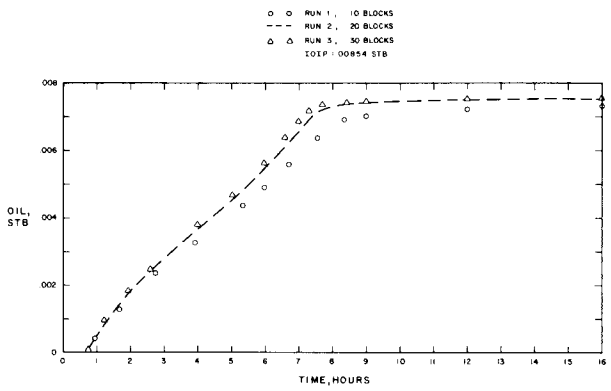

Fig. 5 – Calculated cumulative oil recovery vs. time – Smith-Perkins experiment.

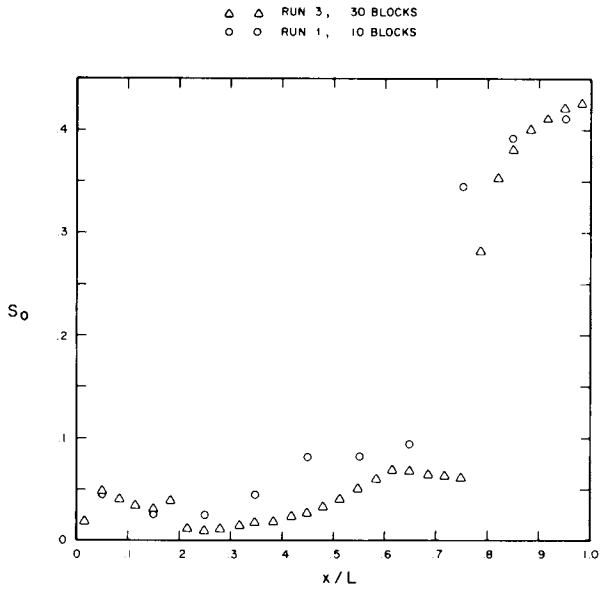

Fig. 6 – Calculated oil saturation profile at 6 hours – Smith-Perkins experiment.

$$A'_o p_{O_2} (\phi \rho_o S_o X_i)^2 e^{-\frac{B}{T}}, \quad \ldots\ldots\ldots\ldots\ldots\ldots (33)$$

where X_i is mole fraction of oil component i in the oil phase. This second-order dependence on oil concentration partially compensates for our neglecting Cf. The value of A'_o was chosen so that the rates of Eqs. 32 and 33, expressed in consistent units, are equal at initial oil-component concentrations.

Reaction stoichiometry and other data listed in Table 1 were obtained from Ref. 9. Since that reference gives no capillary-pressure or relative-permeability data, we used zero P_c and analytical relative permeability curves with exponents of 2.0.

Our one-dimensional model Runs 1, 2, and 3 were made using the data of Table 1 and using 10, 20, and 30 grid blocks, respectively. Figs. 1, 2, and 3 show the agreement between calculated and observed temperature profiles at 2, 4, and 6 hours, respectively. We attribute the discrepancy along the trailing edge to the external heat convection. These figures indicate (1) reasonably good agreement between observed and calculated (20 grid blocks) profiles at all three times, (2) virtually identical calculated results for 20 and 30 grid blocks at each time, and (3) significant but not extreme numerical dispersion in the results calculated using 10 blocks.

Fig. 4 shows calculated and observed effluent oxygen content vs. time. Calculated results using 20 and 30 grid blocks agree quite well with the observed oxygen breakout time, while the results using 10 blocks show effects of numerical dispersion.

Fig. 5 shows a moderate effect of numerical dispersion on calculated oil recovery vs. time for the case of 10 grid blocks. Smith and Perkins reported an estimated figure of 8.8 wt% of the original oil in

place burned. The calculated figure for the 30-block case was 10.38 wt%.

Fig. 6 shows the calculated oil saturation profile at 6 hours for the 10- and 30-block runs. The sharp jump in oil saturation occurs at the leading edge of the sharp temperature profile. A sharp jump from essentially zero to 0.80 to 0.90 in mole fraction of light oil also occurs at this temperature and oil saturation "front."

A favorable aspect of the combustion process frequently emphasized in the literature is the in-situ upgrading of a heavy oil by cracking. Cracking was presumed negligible in this experiment due to the relatively low temperature and light oil. However, an "upgrading" type of effect is still present through distillation or preferential vaporization and recovery of lighter ends. For example, the calculated total oil recovery on a stock-tank-barrel basis was 88.69%. However, the calculated percentages recoveries for $C_6 + C_8 + C_{12}$, C_{20}, and $C_{32} + C_{47}$ were 99.8, 79, and 69%, respectively.

The reaction-rate e^{-Cf} factor used by Smith and Perkins resulted in their numerical model's calculated reaction rates declining very rapidly with increasing fraction of oil burned in the range of $f = 0$ to 0.1. Our second-order reaction gives a much less severe decline in reaction rate with increasing fraction of oil burned. They determined their large rate decrease (large C) from combustion tests in an isothermal tube with no water and an initial oil saturation of 0.15. We feel that that type of test might give a misleading e^{-Cf} factor due to the wetting, low-value oil saturation occupying the tight or small, relatively inaccessible portion of the pore space. This might lead to strongly diffusion-controlled reaction rates. In the actual combustion tube tests, water saturation of 20 to 50% might force the oil into much more accessible (to air) portions of the pore space, resulting in a decrease of diffusion control.

All model runs were performed with midpoint convective weighting ($\theta = 0.5$ in Eq. 12). Use of upstream convective weighting resulted in a significantly greater discrepancy between calculated results for 10, 20, and 30 grid blocks.

Computations for all runs were performed for 18 hours or 0.667 days. Model computing efficiency for the three runs can be summarized as follows.

Run	Number of Grid Blocks	Number of Time Steps	Number of Iterations	Computing Time, CDC 6600 (seconds)
1	10	42	160	83
2	20	53	250	251
3	30	62	330	500

Parrish and Craig Data

Parrish and Craig[11] reported results from wet, forward combustion tests in a vertical adiabatic tube with length and diameter equal to 12 and 1 ft, respectively. Original oil viscosity for their 11 tests reported varies from 2.0 to 2,900 cp at 100°F. Pressure level was 500 to 600 psia.

We feel the data presented by the authors are not sufficiently complete to warrant a serious matching effort. However, we have made a number of model runs seeking qualitative agreement with the experimental temperature profiles reported.

We selected Parrish and Craig's 2,900-cp Test 2 for matching. Five components were represented – water, heavy (original) oil, $N_2 + CO_x$, light (cracked) oil, and oxygen. The two chemical reactions were oxidation and cracking of heavy oil. Coke formation and oxidation were neglected.

Their reported Test 2 experimental conditions are given in the first section of Table 2. Injection rates, time period of initial dry air injection, relative permeability, and kinetic and stoichiometric data were not reported. Table 2 gives the values used for these data. The authors reported experimental temperature profiles at three times for a "typical" COFCAW test.

We present computed results here for two runs. The runs differed in respect to the following data.

Run Number	Heat of Reaction, Oxidation Reaction (Btu/lbm oil)	Rate Constraint, Cracking Reaction
4	16,000	10^6
5	20,000	0.25×10^6

We heated the first 10% of tube length to 500°F at time zero, then injected 20 scf/hr of air at 130°F for 28 hours. Maximum injection pressure was 900 psia, and producing backpressure was 500 psia. The injection well went on injectivity during the period of about 17 to 58 hours due to banking of cold (2,900-cp) oil ahead of the combustion front. Starting at 28 hours and continuing to 96 hours, injection rates were 0.19713 STB [cold-water equivalent (CWE) per day] of water and 480 scf/D of air – an air/water ratio of 2,435 scf/bbl. The authors stated their tests required 30 to 100 hours. Our 4-day run is 96 hours.

Figs. 7 and 8 indicate grid sensitivity through comparison of Run 4 with 10 and 20 grid blocks. The 20-block run calculated a lower injectivity due to sharper oil-bank definition; therefore, the curve of cumulative air injected vs. time for the 10-block run lies somewhat above that for the 20-block run.

Fig. 7 shows peak temperature in each grid block vs. grid block position. The 10- and 20-block runs agree well, with the exception of the blocks in the 0.1 to 0.3 X/L interval, where the 20-block-run peak temperature is less due to lower injection rate during the corresponding time period. The decline in peak temperature with distance traveled reflects a gradual "extinction" of the dry combustion zone upstream of the steam plateau.

Fig. 8 shows reasonably good agreement between oil recovery curves computed with 10 and 20 grid blocks.

The effect of a 25% increase in heat of reaction from Run 4 to Run 5 was one of increased peak temperature and sustaining of the dry combustion zone throughout the duration of the run. That is,

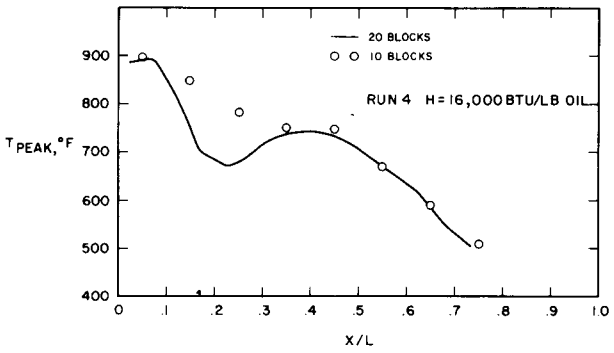

Fig. 7 – Calculated peak temperature vs. distance along tube – Parrish and Craig COFCAW experiment.

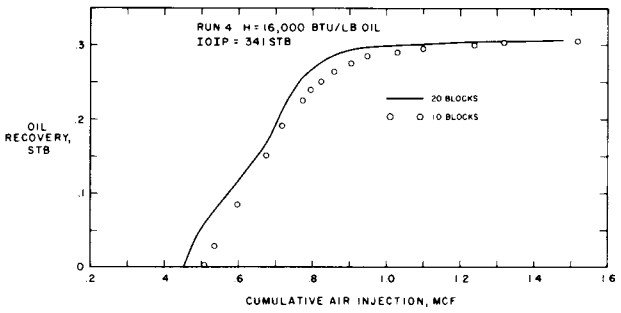

Fig. 8 – Calculated oil recovery vs. cumulative air injection – Parrish and Craig COFCAW experiment.

TABLE 2 – DATA FOR PARRISH AND CRAIG COFCAW TEST 2

Data From Ref. 11

Oil gravity, °API	13.5
Oil viscosity at 100°F, cp	2,900
Initial S_w, S_o, S_g	0, 0.712, 0.228
Initial cell temperature, °F	130
Air/water ratio, scf/bbl	2,435
Porosity, percent	30
Permeability, md	1,000
Tube length, ft	12
Tube diameter, in.	12
Initial pressure (outlet backpressure), psig	500

Viscosity Data

$\mu_{22} = 0.0002\, e^{9,237/T}$
$\mu_{33} = 0.0002127\, T^{0.7030}$
$\mu_{42} = 0.01044\, e^{2,618/T}$
$\mu_{43} = 0.01$
$\mu_{53} = 0.0002196\, T^{0.721}$

K-Value Data

$K_{v23} = 0$
$K_{v43} = (1.157 \times 10^6/p)\, e^{-9,933/T}$

Additional Data

Rock heat capacity, Btu/cu ft rock-°F	35
Thermal conductivity, ft-D-°F	3
Initial mole fractions $X_1 = 1.0, X_2 = 1.0, X_3 = 0.9919, X_4 = X_5 = 0$	
Number of grid blocks	10 and 20
Number of components	5
Number of reactions	2

First 10% of tube length raised to 520°F to start ignition

Reaction Data

C_i denotes component i

Component I	Molecular Weight	p_c	T_c(°R)	c_I	β_I	C_{PI} (Btu/lbm)
1. H_2O	18	3,206	1,165.4			
2. Heavy oil	300	50.7	1,598	10^{-5}	0.38×10^{-3}	0.5
3. $N_2 + CO_x$	32	750	350			0.226
4. Light oil	170.3	264.6	1,184.9	10^{-5}	0.38×10^{-3}	0.5
5. O_2	32	730	277.9			0.24

$v^o_{22} = 0.01642$ cu ft/lbm
$v^o_{42} = 0.01874$ cu ft/lbm
Stock-tank oil densities (lbm/cu ft) Components 2 and 4 = 61.15 and 53.35

Reaction r	Stoichiometry
1.	$C_2 + 32.143\, C_5 \rightarrow 21.429\, C_1 + 21.429\, C_3$
2.	$C_2 \rightarrow 1.761\, C_4$

	Rate Constant $A_r \times 10^{-6}$	Activation Energy E_r
1.	42.25	18,214
2.	0.25	16,000

Heat of oxidation, Reaction 1 = 16,000 Btu/lbm oil for Run 4
= 20,000 Btu/lbm oil for Run 5
Heat of cracking reaction = 20,000 Btu/lbm mol oil

Relative Permeability and Capillary Pressure Data

Same as in Table 1

Injection Production Data

Injection rate: 480 scf/D air at 130°F
Production on deliverability at 500 psig

peak temperature did not decline with distance traveled in Run 5. Also, at the higher heat of reaction, reduction of the cracking reaction-rate constant from 10^6 to 0.25×10^6 caused a moderate increase in calculated peak temperature.

The dashed curves in Fig. 9 are plots of the "typical" COFCAW test presented by Parrish and Craig. The three times of the experimental, dashed profiles are "start COFCAW," "steam breakthrough," and "combustion zone breakthrough." The times corresponding to the three Run 5 calculated profiles are 28, 57, and 89.5 hours, respectively.

For Run 5, the calculated oil recovery was 93.6% compared with Parrish and Craig's reported 87.9%. Calculated oil burned was 7.15% compared with Parrish and Craig's reported 7.88% of initial oil in place. The calculated figures are a little low in that combustion was continuing ($S_o = 0.15$) in the 10th block at the end of the run. Reported and calculated air/recovered-oil ratios are 6,020 and 5,166 scf/bbl, respectively.

On a volumetric stock-tank-barrel basis, 24% of the oil recovery calculated in Run 5 was Light Component 4. One hundred percent of the light oil formed by cracking was produced, since final oil saturation was zero and we included no oxidation reaction for the light oil.

Run 5 used 10 grid blocks and required 108 CDC 6600 seconds, 61 time steps, and 302 total iterations for the 4 days of real time.

Crookston, Culham, and Chen Problem

Crookston *et al.*[2] simulated oxygen injection into a one-dimensional, 200°F reservoir 164 ft long, 115 ft wide, and 21 ft thick. Reaction and fluid-property data were estimated from values given in the literature. Their four reactions represented oxidation of light and heavy oil components, cracking of heavy oil, and oxidation of coke.

Table 3 lists our model input data for this problem. Our data are identical to those of Crookston *et al.* with the following exceptions. Our oil relative permeability curve is only similar to theirs. They used a multiplicative factor of $1 - (n_c/n_{cmax})^5$ in their cracking reaction-rate expression, with $n_{cmax} = 0.07692$ lbm mol/cu ft of formation. We used no maximum equivalent $(S_4)_{max}$, since our calculated coke laydown did not exceed their n_{cmax}.

As given in Table 3, the problem includes the six components water, heavy oil, N_2-CO_x, coke, oxygen, and light oil. Thus, our simulation required simultaneous solution of six primary equations – one energy balance plus five component mass balances – with the immobile coke mass balance treated as a constraint equation.

Crookston *et al.* used propane and dodecane properties for light and heavy oils, respectively, with an increased viscosity for dodecane. At 200°F, the liquid-component viscosities of light and heavy oil are 0.089 and 139 cp, respectively.

Crookston *et al.* described their calculated results in some detail both verbally and graphically. Since our results agree very closely with theirs in all respects, we will not repeat the extended discussion and figures.

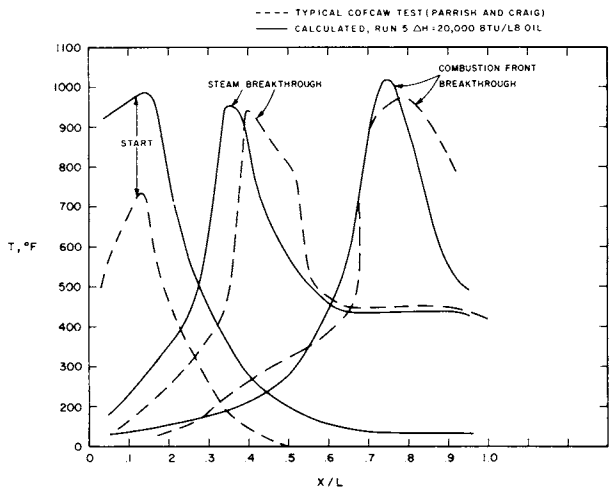

Fig. 9 – Calculated and experimental COFCAW temperature profiles.

Table 4 summarizes the agreement between the two sets of calculated results. Oil recovery is volumetric oil recovery expressed as a percentage of initial oil in place. Stock-tank oil densities are 45.313 and 23.633 lbm/cu ft for heavy oil and light oil, respectively, at 72°F and 14.7 psia. Initial water and oil in place are 5,168 and 12,590 STB, respectively. The light oil recovery is expressed as volumetric percentage of total oil recovery. Heat loss (to overburden) is expressed as a percentage of total heat of reactions. Combustion-front velocity is calculated as $0.7(164)/(t_9\ t_2)$, where t_i is time in days of the temperature peak in grid block i and 164 ft is the system length. T_{pavg} is average peak temperature of Cells 2 through 9, inclusive, peak temperatures. Water recovery is expressed as a percentage of initial water in place. Heat of reaction is total heat of all reactions. Computing time is in CDC 6600 CPU seconds.

Table 4 shows fairly good agreement between the Crookston *et al.* results and our Run 6 results. Both we and they calculated a steam zone or plateau throughout the system by the time the first cell peaked in temperature. The reason for this very rapid steam-zone development is the passage of unreacted oxygen throughout the system in the first 10 to 20 days prior to first-block spontaneous ignition. This oxygen reacts sufficiently throughout the system to raise temperature throughout to about 300°F.

Energy balance and component material balances for Run 6 were excellent, ranging only from 0.9999 to 1.0001.

Crookston *et al.* reported a computing time for this problem of 1,071 seconds on an IBM 370/168 computer. Run 6 required 242 seconds on a CDC 6600 computer. CDC 6600 computer times are about 2.2 times larger than IBM 370/168 times for our steamflood model.[6] Much of the difference between the computer time reported by Crookston *et al.* and that reported here reflects the fact that their for-

TABLE 3 – DATA FOR CROOKSTON *ET AL.* ONE-DIMENSIONAL FIELD-SCALE PROBLEM

Reservoir length, ft	164
Reservoir width, ft	115
Reservoir thickness, ft	21
Permeability, md	4,000
Porosity	0.38
Rock heat capacity, Btu/cu ft rock-°F	35
Thermal conductivity, Btu/ft-D-°F	1.6
Overburden thermal conductivity, Btu/ft-D-°F	1.6
Overburden heat capacity, Btu/cu ft overburden-°F	35
T_i, °F	200
p_i, psia	65

Initial water, oil, gas saturation = 0.2, 0.5, 0.3
Initial mole fraction $X_1 = 1.0, X_2 = 1.0, X_3 = 0.806, X_4 = X_5 = X_6 = 0$

Number of grid blocks (one-dimensional)	10
Number of components	6
Number of reactions	4

Component l	Molecular Weight	p_c	T_c(°R)	c_l	β_l	C_{pl} (Btu/lbm)
1. H_2O	18	3,206.2	1,165.4			
2. Heavy oil	170	264.6	1,184.9	10^{-5}	0.000382	$0.34 + 0.0003547\,T$
3. CO_2	44	1,073	547.7			0.25
4. Coke	13					0.3
5. O_2	32	730	277.9			0.24
6. Light oil	44	615.9	665.6	2.2×10^{-4}	0.000769	$-1.1843 + 0.003452\,T$

K-Value

$$K_{v23} = (184{,}900/p)\, e^{-6{,}739/(T-167.1)}$$
$$K_{v63} = (130{,}700/p)\, e^{-3{,}370/(T-45.29)}$$

Reaction Data

C_i denotes component i

$$v^o_{22} = 0.0235 \text{ cu ft/lbm}$$
$$v^o_{62} = 0.05 \text{ cu ft/lbm}$$
$$v^o_{44} = 0.0125 \text{ cu ft/lbm}$$

Viscosity Data

$$\mu_{22} = 0.0003624\, e^{8{,}485/T}$$
$$\mu_{23} = 0.3926 \times 10^{-5}\, T^{1.102}$$
$$\mu_{33} = 0.0002127\, T^{0.702}$$
$$\mu_{53} = 0.0002196\, T^{0.721}$$
$$\mu_{62} = 0.02083\, e^{959.6/T}$$
$$\mu_{63} = 0.2166 \times 10^{-4}$$

Reaction r	Stoichiometry
1	$C_2 + 18\,C_5 \rightarrow 12\,C_3 + 13\,C_1$
2	$C_6 + 5\,C_5 \rightarrow 3\,C_3 + 4\,C_1$
3	$C_2 \rightarrow 2\,C_6 + 4.67\,C_4 + 1.33\,C_3$
4	$C_4 + 1.25\,C_5 \rightarrow C_3 + 0.5\,C_1$

	Rate Constant $A_r \times 10^{-6}$	Activation Energy E_r	Heat of Reaction H_{r1} (Btu/mol first reactant)
1	1.0	18,500	3.49×10^6
2	1.0	18,500	0.948×10^6
3	0.3	16,000	20,000
4	1.0	13,000	0.225×10^6

Relative Permeability and Capillary Pressure Data

$$S_{wi} = S_{wir} = 0.2$$
$$S_{orw} = 0.3$$
$$S_{org} = 0.09$$
$$S_{gc} = S_{gr} = 0.05$$
$$k_{rwro} = 0.25$$
$$k_{roiw} = 1.0$$
$$k_{rgro} = 0.7$$
$$n_w = n_{ow} = n_{og} = 3$$
$$n_g = 1$$
$$P_{cwo} = 0.75 - 1.5\,\hat{S}_w$$
$$P_{cgo} = 5.45 - 8.45\,\hat{S}_L$$

Injection/Production Data

Oxygen injection rate: 300 lbm mol/D, 200°F
Production on deliverability at 60 psia
Productivity index: 300 RB-cp/D-psi

TABLE 4 – COMPARISON OF CROOKSTON *ET AL.* WITH RUN 6 RESULTS FOR EXAMPLE ONE-DIMENSIONAL FORWARD COMBUSTION PROBLEM

	Crookston *et al.*	Run 6
Oil recovery, %	97	97.18
Light oil, %	30	27.7
Heat loss, %	27	26
Velocity, ft/D	1.2	1.35
Water recovery, %	119	118.2
T_{pavg}, °F	849	836
Heat of reaction, Btu $\times 10^{-10}$	0.7925	0.7183
Computing time, seconds	1,071*	242**
Number of time steps	764	122
Number of iterations	3,056	530
Average Δt, days	0.1965	0.122
Time Step Controls		
Saturation	0.1	0.4
Mole fraction	0.2	None
Pressure, psi	90	20
Temperature, °F	30	80

Cell	Peak Temperature [°F (days)]	
1	600(33.3)	534(32.3
2	775(44.9)	728(42.1)
3	855(57.5)	861(52.7)
4	850(71.5)	878(65.9)
5	868(85.9)	924(79.9)
6	820(99)	816(92)
7	875(113.1)	824(103)
8	870(126.6)	836(116)
9	880(140.5)	822(127)
10	780(150.2)	653(137)

*IBM 370/168.
**CDC 6600.

TABLE 5 – SENSITIVITY RUN RESULTS – ONE-DIMENSIONAL FORWARD COMBUSTION

Run	Oil Recovery (%)	Light Oil (%)	Heat Loss (%)	Velocity (ft/D)	Water Recovery (%)	T_{pavg} (°F)	Heat of Reaction (Btu × 10^{-10})	Time (days)	
7	93.5	19.9	34.9	1.39	123.8	622	0.3990	91.5	Base case
8	93.7	20.3	35.8	1.36	123.4	633	0.3965	88.1	$k = 0.5x$
9*	74	13.4	30.1	2.23	129.2	475	0.2737	87.4	$\phi = 0.63x$
10	93.9	19.7	29.2	1.43	122.7	640	0.3842	88.7	$\lambda_{OB} = 0.5x$
11	94.5	18.9	34.9	1.47	120.9	628	0.3918	80.6	$(H_1)_1 = 1.2x$
12	93.9	19.1	35.0	1.51	122.4	662	0.4136	87.4	$(H_4)_1 = 1.2x$
13	92.9	14.0	40.6	1.31	122.7	647	0.3615	65.3	$E_1 = 0.8x$
14	99.2	86.1	52.9	0.44	137.9	1,244	0.869	160	$E_3 = 0.8x$
15**	89.4	20.4	43.8	0.52	132.4	646	0.5039	146	$E_4 = 1.77x$
16	93.5	17.6	35.7	1.31	122.6	606	0.3754	75.9	$A_1 = 2x$
17	95.2	30.7	37.1	1.19	124	705	0.4484	96	$A_3 = 2x$
18	93.7	20.0	34.4	1.55	123.2	608	0.3920	89.6	$A_4 = 2x$
19	93.4	18.7	34.3	1.58	123.4	605	0.3894	90	$n_{ow} = n_{og} = 2$
20	93.5	20.6	34.8	1.35	123.9	631	0.4040	91.4	$n_{ow} = n_{og} = 4$
21	93.4	19.6	35.3	1.44	123.8	621	0.3985	91.9	$P_{cwo} = P_{cgo} = 0$
22	94.6	55.6	46.6	0.71	130.1	1,021	0.6979	143	$(K_{V4})_2 = 8{,}000$
23	93.4	18.9	34.4	1.57	123.5	604	0.3913	89.7	$(K_{V4})_6 = 5{,}000$

*First block did not "ignite." Spontaneous ignition occurred in Block 2.
**Coke was not completely burned out of Cells 1 and 2.

mulation required about 764 time steps compared with 122 for Run 6. Their larger computing time per block step reflects, at least in part, their direct solution of nine primary equations compared with our six primary equations.

We feel the considerably smaller number of time steps in our Run 6 is primarily due to the completely implicit formulation, which allows larger steps. We have noted very little time truncation error in forcing our runs to use smaller time steps.

Sensitivity Runs

A number of one-dimensional sensitivity runs were made using the Crookston *et al.* data. These runs were made to indicate which data are "important" in the sense of having a significant influence on calculated results. The results serve as a guide for history-matching efforts in that they indicate the types of response to changes in various input-data variables. The utility of the sensitivity-run results is limited because they are only applicable to the Crookston *et al.* data and do not reflect two- or three-dimensional flow effects.

The base case (Run 7) is a reservoir 82 ft long, 115 ft wide, and 21 ft thick. The 82-ft length is represented by five 16.4-ft grid blocks. A well productivity index of 1,328 was used together with the data listed in Table 3.

Base Run 7 results are tabulated in Table 5. T_{pavg} is the average of peak temperatures in Cells 2 through 4. Velocity is $2 \times 16.4/(t_4 - t_2)$, where t_i is time of peak temperature in Cell 1. Time tabulated in Table 5 is the time at which the last cell (Cell 5) peaked in temperature; oil recovery was complete at some time prior to that time in all cases. The notation in the last column of Table 5 (e.g., $E_1 = 0.8$) means that activation energy of Reaction 1 is 0.8 times the base-case value. K_{V4} is defined for heavy and light oil Components 2 and 6 by

$$K_i = (K_{V2i}/p)\, e^{-\frac{K_{V4i}}{T - K_{V5i}}},$$

where K_i is the equilibrium K-value ($y_i = K_i x_i, x_i$ = oil-phase mole fraction, and y_i = gas-phase mole fraction) of component i. Thus, increasing the K_{V4} value decreases the component volatility. Base-case values of K_{V4} for Components 2 and 6 are 6,739 and 3,370, respectively.

A number of runs made are unreported in Table 5 because of insensitivity of results to (1) 20% increases in component or rock specific heats, (2) 50% reduction in oil-component thermal expansion coefficient, and (3) change from 44 to 32 of CO_x gaseous Component 3 molecular weight.

Run 8 indicates little sensitivity to permeability in the range of 2,000 to 4,000 md. Actually, reduced permeability may have a pronounced effect if it is reduced to a value low enough to increase reservoir pressure significantly and, hence, reaction rate.

Run 9 indicates a pronounced effect of lowered porosity. Reaction rate decreases due to smaller reactant concentrations and oil recovery falls from 93.5 to 74% as porosity is decreased from 0.38 to 0.24. Also, of course, more rock is associated with a given pore-space volume as porosity is decreased.

Reduction of overburden thermal conductivity by a factor of two reduces the heat loss moderately but has little effect on oil recovery and peak temperature (Run 10).

Runs 11 and 12 show that a 20% increase in coke-oxidation heat of rection has a greater effect than a 20% increase in the direct-oxidation heat of reaction. Run 13 shows increased heat loss and peak temperature caused by decreased activation energy of the direct-oxidation Reaction 1. Run 14 shows that a decreased cracking-reaction activation energy doubles the peak temperature to 1,244°F and gives a much lower combustion-zone velocity and higher (volumetric) oil recovery, with light-oil volumetric fraction in recovered oil rising from 19.9 to 86.1. Increasing the coke-oxidation activation energy by 54% (Run 15) moderately increases peak temperature and heat loss. Runs 16 through 18 indicate a greater

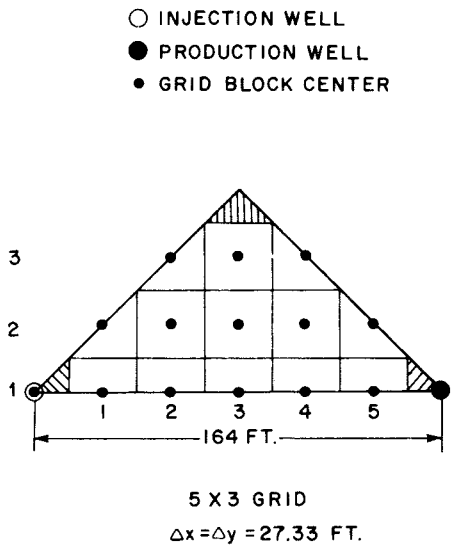

Fig. 10 – One-eighth of a five-spot grid.

	i=2	i=3	i=4	
k=1	640.3 (48.0)	869.9 (144.0)	1146.8 (214.0)	TEMP, °F (TIME, DAYS)
k=2	608.5 (71.2)	431.6 (119.0)	994.5 (285)	
k=3	396.5 (144.0)			
k=4				

Fig. 11 – Peak temperature of a 5 × 4 wedge – Run 25.

sensitivity to cracking reaction-rate constant than to direct-oxidation or coke-oxidation reaction-rate constants. The sensitivities noted here should be viewed with the knowledge that only about 3% of the oil is consumed by the direct-oxidation reaction for the base-case data.

Oil relative permeability was increased considerably in Run 19 and decreased in Run 20. Heat loss, light oil production, velocity, and peak temperature increase slightly with decreased oil relative permeability. Run 21 shows a negligible effect of capillary pressure.

Run 22 shows that a reduced volatility of heavy oil Component 2 significantly increases peak temperature and decreases velocity. Percentage of light oil in the recovered oil rises from 19.8 to 55.6 and total heat of reaction increases by 50%. Run 23 shows a much smaller effect of reduced volatility of light oil Component 6. Component 6 is so volatile in the base-case data that virtually none of it is oxidized by Reaction 2. That is, light oil is vaporized nearly as rapidly as it is formed and is carried in the gas phase downstream from the combustion front.

Three-Dimensional Run

Runs 24 and 25 simulated one-eighth of a 1.24-acre five-spot with an injection/production well distance of 164 ft and formation thickness of 80 ft. Initial reservoir pressure and temperature were 500 psia and 200°F. Air injection was 336.8 Mcf/D at 500°F for 10 days with the production well produced on deliverability at 500 psia. Starting at 10 days, 93.18 STB/D of water were injected along with 336.8 Mcf/D of air at 200°F for an air/water ratio of 2,615 scf/bbl.

Four 20-ft layers were used with an upper gas-filled layer and lower water-saturated layer. Initial saturations were as follows:

Layer	S_{wi}	S_{oi}	S_{gi}
1	0.2	0.09	0.71
2	0.2	0.75	0.05
3	0.2	0.75	0.05
4	1.0	0	0

The injection completed in Layer 3 only while the producer was completed in Layers 2 and 3, with a total well productivity index of 1,123 split evenly between the two layers. Initial gas composition was 77.44% N_2 and 20% O_2, with the balance water vapor. Initial water and oil in place were 14,050 and 13,590 STB, respectively. The remaining data were identical to those given in Table 3.

Three-dimensional Run 24 utilizes a 5 × 3 × 4 grid, with $\Delta x = \Delta y = 27.33$ ft and $\Delta z = 20$ ft. Fig. 10 is an areal view of this grid illustrating the parallel orientation[14] with the x axis coincident with the line joining the wells. The cross-hatched small "tip" blocks are eliminated, with their pore volumes included in their neighbor blocks.[4-6]

Run 25 is a 5 × 1 × 4 two-dimensional, wedge-shaped cross section with variable width reflecting the triangular one-eighth five-spot shape. Δx is 32.9 ft, and except for the two-dimensional variable-width aspect, all data are identical to those for the three-dimensional Run 24.

The runs were terminated at 300 days. For the three-dimensional Run 24 at that time, oil production rate had declined to less than 5 STB/D and instantaneous WOR and GOR were 15.5 STB/STB and 82.5 Mcf/STB, respectively.

The initial gas-filled layer along the top of the reservoir resulted in a strong "overburn," as indicated by the peak temperatures and time noted in Fig. 11. Peak temperatures less than 500°F reflect the presence of liquid water and corresponding constraint on temperature.

In both runs the upper layer burned dry, with maximum coke saturations reaching the 5% level. Oil was pushed into the upper layer, reaching saturations as high as 60% compared with the original 9%. Oil also was pushed downward into the aquifer layer, reaching saturations as high as 22%.

Calculated oil recovery at 300 days for the three-dimensional Run 24 was 52.3%. On a volumetric basis, light oil formed by cracking was 28.5% of this total recovery. Calculated oil production rate peaked at 61 STB/D at 41 days and averaged 32 STB/D over the first 200 days and 7.6 STB/D during the period 200 to 300 days.

Fig. 12 compares calculated heat loss and oil recovery Runs 24 and 25. The two-dimensional run calculates somewhat higher oil recovery but approximates the three-dimensional run moderately well.

Table 6 summarizes the model computing efficiency for Runs 24 and 25. The three-dimensional run using 52 active blocks required 55 minutes of CDC 6600 computer time. The automatic time-step selection in the runs used maximum changes per step in saturation, pressure, and temperature of 0.2, 100 psia, and 80°F, respectively.

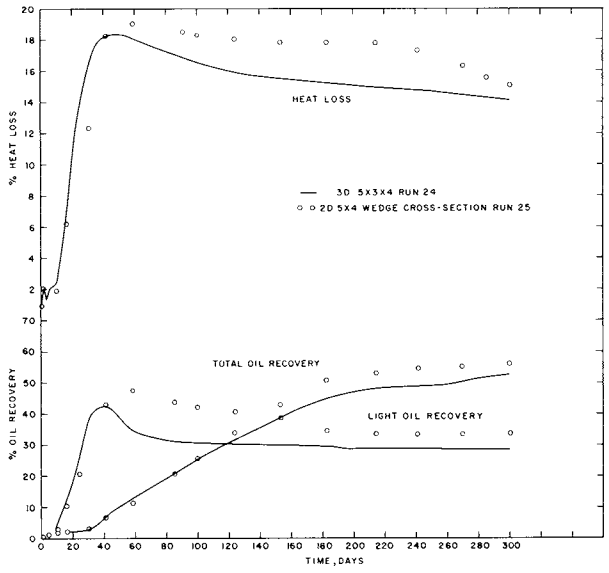

Fig. 12 – Comparison of oil recovery with heat loss for Runs 24 and 25.

Summary

The formulation described here for numerical simulation of in-situ combustion processes is more general than previously described models. The number and identities of components, number of reactions and corresponding reactants, products, and stoichiometry are not limited or "hard cored" but rather are specified through input data. Vaporization/condensation phenomena are treated with maximum flexibility by allowing any component to be distributed among all phases.

One aspect of the formulation's generality is the applicability to thermal problems ranging from single-component geothermal problems to multicomponent steamflood and in-situ combustion problems, without recourse to different model versions.

The model uses an improved variable substitution method using single set of "master-phase" mole fractions. The formulation is implicit, reflecting our belief that computing expense or arithmetic for most practical problems will decrease as the formulation is rendered more implicit. The formulation takes maximum advantage of constraint equations to reduce the number of primary equations requiring the relatively expensive direct solution by Gaussian elimination.

Model results agree moderately well with experimental results from two independent, published, laboratory adiabatic-tube studies. However, the second study did not present sufficient measured data to attach quantitative significance to the model's match.

The model required less than 1 hour of CDC 6600 computer time to solve a six-component, 5 × 3 × 4, three-dimensional, wet forward combustion example problem representing one-eighth of a five-spot.

The model results agreed very well with those calculated by Crookston *et al.* for a one-dimensional, field-scale, forward combustion problem involving six components. We attribute our significantly lower computing time for this problem to our implicit formulation and minimization of primary equations requiring direct solution.

A number of sensitivity runs using data for the above-mentioned problem indicate that calculated combustion behavior is strongly dependent on relatively few of the many model input-data values.

Nomenclature

A = cross-sectional area normal to flow, sq ft (m^2)

TABLE 6 – COMPUTING TIMES AND TIME-STEP SIZES FOR TWO-DIMENSIONAL 5 × 4 AND THREE-DIMENSIONAL 5 × 3 × 4 RUNS

Run	Number of Active Blocks	Time (days)	Cumulative Number of Time Steps	Cumulative Number of Iterations	Cumulative Time*	Cumulative Time per Block Step	Average Time Step (days)**
24	52	200	107	464	2,944		1.87
		300	118	517	3,280	0.535	9.1
25	20	200	88	385	525		2.27
		300	107	477	651	0.304	5.26

*Cumulative computer time, CDC 6600 CPU seconds.
**Average time step, days, in 0- to 200-day or 200- to 300-day intervals.

A_r = reaction-rate constant for reaction r (Eq. 15)

c_I = compressibility of component I (Eq. A-5), vol/vol-psi (1/kPa)

C_{IJ} = coefficients in matrix of linearized model equations

C^o_{PI} = ideal gas-state heat capacity of component I, Btu/lbm mol-°F (kJ/kmol·K)

E_r = activation energy for reaction r, cal/g mol (kJ/kmol)

H_{IJ} = partial enthalpy of component I in phase J, Btu/lbm mol (kJ/kmol)

H^o_I = ideal gas-state enthalpy of component I, Btu/lbm mol (kJ/kmol)

H_J = enthalpy of phase J, Btu/lbm mol (kJ/kmol)

H_r = heat of reaction r for grid block Btu/D (kJ/d)

H_{r1} = heat of reaction r of first reactant, Btu/lbm mol (kJ/kmol)

H^{SL} = enthalpy of saturated liquid, Btu/lbm mol (kJ/kmol)

H^{SV} = enthalpy of saturated vapor, Btu/lbm mol (kJ/kmol)

ΔH_{vb} = heat of vaporization at boiling point, Btu/lbm mol (kJ/kmol)

I = component index

J = phase index

J_I = primary or master phase for component I

k = absolute permeability, md × 0.00633

k_i = value of k read as input data

k_{rg} = relative permeability to gas

k_{rJ} = relative permeability to phase J, fraction

k_{ro} = oil relative permeability, fraction

k_{rw} = water relative permeability, fraction

k_{rgro} = relative permeability to gas at residual liquid saturation

k_{rog} = relative permeability to gas in a gas/oil system with connate water

k_{roiw} = relative permeability to oil at irreducible water saturation

k_{row} = relative permeability to oil in an oil/water system

k_{rwro} = relative permeability to water at residual oil saturation

K_{vIJ} = equilibrium K-value for component I in phase J

$K_{V1} - K_{V5}$ = coefficients for calculation of K_{vIJ}

ℓ = iteration number ln to base e

L = distance between adjacent grid block centers, ft (m)

K_v = heat of vaporization, Btu/lbm mol (kJ/kmol)

M_f = reservoir-rock heat capacity, Btu/cu ft rock-°F (kJ/m^3 rock-K)

M_I = molecular weight of component I

M_J = molecular weight of phase J

n_g = exponent on gas saturation for k_{rg}

$n_{j,r}$ = order of reaction r in the jth reactant

n_{og} = exponent on oil saturation for k_{rog}

n_{ow} = exponent on oil saturation for k_{row}

n_w = exponent on water saturation for k_{rw}

$N = N_P + N_C + 2$

N_C = number of components

N_P = number of phases

N_R = number of chemical reactions

$N_{R,r}$ = number of reactants in reaction r

p = gas-phase pressure, psia (kPa)

p_c = critical pressure, psia (kPa)

p_{cI} = critical pressure of component I, psia (kPa)

p_g = gas-phase pressure

p_i = original reservoir pressure

p_j = phase J pressure, $p + P_{cJ}$

p_k = pressure in grid block, layer k, at well, psia (kPa)

p_o = oil-phase pressure, $p - P_{cgo}$

p_w = water-phase pressure, $p - P_{cgo} - P_{cwo}$

p_{wb} = wellbore flowing pressure, psia (kPa)

p_{wbk} = wellbore flowing pressure opposite center of layer k, psia (kPa)

P_{cgo} = gas/oil capillary pressure, $p_g - p_o$

P_{cJ} = phase J capillary pressure, $p_J - p$

P_{cwo} = water/oil capillary pressure, $p_o - p_w$

P_m or P_j = mth or jth unknown (Eq. 7)

PI_k = time-dependent productivity index of layer k, res cu ft-cp/D-psi (res m^3)

q_I = production rate of component I from grid block, mol/D

q_{Ik} = rate of production of component I from layer k, mol/D

q_{Ir} = rate of creation of component I in grid block due to reaction r, mol/D

q_{Jk} = rate of production of phase J from layer k, res cu ft/D (res m^3/d)

$\dot{Q}_H$ = production rate of enthalpy from grid block association with fluid production, Btu/D (kJ/d)

$\dot{Q}_{Hk}$ = rate of production of enthalpy from layer k, Btu/D (kJ/d)

$\dot{Q}_{HL}$ = heat-loss rate to overburden from grid block, Btu/D (kJ/d)

R = gas-law constant, 1.987 Btu/lbm mol-°R (kJ/kmol·K)

R_r = rate of reaction r in grid block, lbm mol (kmol) of first reactant/D

s_{ir} = stoichiometric coefficient of ith participant in reaction r

$S_{\bar{g}c}$ = critical gas saturation

S_{gr} = residual gas saturation

$(S_g)_{max}$ = maximum historical gas saturation in a grid block

S_J = saturation of phase J

$\hat{S}_J = S_J/(1 - S_4)$

S_L = liquid saturation, $1 - S_g$

$\hat{S}_L = S_L/(1 - S_4)$

S_{org} = residual oil saturation to gas

S_{orw} = residual oil saturation to water

S_{wi} = connate water saturation, fraction

S_{wir} = irreducible water saturation, fraction

S_4 = solid phase saturation

$(S_4)_{max}$ = maximum allowed coke saturation (Eq. 13)

T = temperature, °R (K)

T_b = boiling point, °R (K)

$T_{br} = T_b/T_c$

T_c = critical temperature, °R (K)

T_i = original reservoir temperature

T_r = reduced temperature, T/T_c

T_1 or T_2 = temperature of Grid Block 1 or 2

U_J = grid block volume, $\Delta x \cdot \Delta y \cdot \Delta z$, cu ft ($m^3$)

v_{IJ} = partial volume of component I in phase J, cu ft/mol (m^3/kmol)

v^o_{IJ} = see Eq. A-5

v_J = specific volume of phase J, cu ft/mol (m^3/kmol)

V = grid-block volume, $\Delta x \cdot \Delta y \cdot \Delta z \cdot$, cu ft ($m^3$)

x_{IJ} = mole fraction of component I in phase J

Δx = grid-block dimension in x direction, ft (m)

X_I = mole fraction of component I in component I's primary base

Δy = grid-block dimension in y direction, ft (m)

z = gas-phase supercompressibility factor

Δz = grid-block dimension in z direction, ft (m)

Z = subsea depth measured positively vertically downward, ft (m)

Z_k = subsea depth to center of layer k at well

Z_1 or Z_2 = subsea depth to center of Grid Block 1 or 2

$\Delta Z = Z_1 - Z_2$

β_I = thermal expansion coefficient for component I (Eq. A-5), vol/vol-°F (1/K)

γ_J = specific weight of phase J, psi/ft (kPa/m)

γ_{Jk} = value of γ_J in layer k

γ_{wb} = wellbore fluid gradient, psi/ft (kPa/m)

θ = weight factor for interblock enthalpy

λ = thermal conductivity (Eq. A-1), Btu/ft-D-°F (W/m·K)

λ_i = value of λ read as input data

λ_{ob} = overburden thermal conductivity

μ_{IJ} = partial viscosity of component I in phase J, cp (Pa·s)

μ_J = viscosity of phase J, cp (Pa·s)

ρ_J = density of phase J, mol/cu ft (kmol/m^3)

τ = fluid-flow transmissibility, kA/L, res cu ft-cp/D-psi (res m^3)

τ_c = heat-conduction transmissibility, $\lambda A/L$

τ_R = radiation transmissibility, $\lambda \alpha_3 A/L$

ϕ = porosity, fraction

Superscript

ℓ = iteration number

Subscripts

i = x-direction grid block index

i_{jr} = component number of jth reactant in reaction r

I = component number

j = y-direction grid block index

J = phase number

k = z-direction grid block index

m_{jr} = phase of jth reactant in reaction r

n = time-step level

r = reaction number

Difference Notation

X is any quantity or arithmetic expression.

$$\delta X = X_{n+1} - X_n ,$$

$$\delta X \cong X_{n+1} - X^{\ell}$$

or

$$\delta X = X^{\ell+1} - X^{\ell} ,$$

where the $(\ell+1)$th iterate, $X^{\ell+1}$, is an approximation to X_{n+1}.

$$\Delta X = X_1 - X_2 ,$$

where Subscripts 1 and 2 refer to adjacent Grid Blocks 1 and 2.

$$\Delta(\tau \Delta X) \equiv \Delta_x(\tau_x \Delta_x X) + \Delta_y(\tau_y \Delta_y X) + \Delta_z(\tau_z \Delta_z X) .$$

$$\Delta_x(\tau_x \Delta_x X) \equiv \tau_{xi+1/2}(X_{i+1} - X_i) - \tau_{xi-1/2}(X_i - X_{i-1}) ,$$

where $\tau_{xi+1/2}$ is x-direction transmissibility for flow between Grid Blocks i and $i + 1$.

References

1. Ali, F.S.M.: "Multiphase, Multidimensional Simulation of In-Situ Combustion," paper SPE 6896 presented at SPE 52nd Annual Technical Conference and Exhibition, Denver, Oct. 9-12, 1977.

2. Crookston, H.B., Culham, W.E., and Chen, W.H.: "Numerical Simulation Model for Thermal Recovery Processes," *Soc. Pet. Eng. J.* (Feb. 1979) 37-58; *Trans.*, AIME, **267**.
3. Youngren, G.K.: "Development and Application of an In-Situ Combustion Reservoir Simulator," *Soc. Pet. Eng. J.* (Feb. 1980) 39-51.
4. Coats, K.H., George, W.D., Chu, Chieh, and Marcum, B.E.: "Three-Dimensional Simulation of Steamflooding," *Soc. Pet. Eng. J.* (Dec. 1974) 573-592; *Trans.*, AIME (1974) **257**.
5. Coats, K.H.: "Simulation of Steamflooding With Distillation and Solution Gas," *Soc. Pet. Eng. J.* (Oct. 1976) 235-247.
6. Coats, K.H.: "A Highly Implicit Steamflood Model," *Soc. Pet. Eng. J.* (Oct. 1978) 369-383.
7. Price, H.S. and Coats, K.H.: "Direct Methods in Reservoir Simulation," *Soc. Pet. Eng. J.* (June 1974) 295-308; *Trans.*, AIME, **257**.
8. Redlich, O. and Kwong, J.N.S.: "On the Thermodynamics of Solutions. V. An Equation of State. Fugacities of Gaseous Solutions," *Chem. Rev.* (Feb. 1949) **44**, 233-244.
9. Smith, F.W. and Perkins, T.K.: "Experimental and Numerical Simulation Studies of the Wet Combustion Recovery Process," *J. Cdn. Pet. Tech.* (July/Sept. 1973) 44-54.
10. Reid, R.C., Prausnitz, J.M., and Sherwood, T.K.: *The Properties of Gases and Liquids*, third edition, McGraw-Hill Book Co. Inc., New York City (1977).
11. Parrish, D.R. and Craig, F.F. Jr.: "Laboratory Study of a Combination of Forward Combustion and Waterflooding – The COFCAW Process," *J. Pet. Tech.* (June 1969) 753-761; disc., *J. Pet. Tech.* (July 1969) 801-802; *Trans.*, AIME, **246**.
12. Braden, W.B.: "A Viscosity-Temperature Correlation at Atmospheric Pressure for Gas-Free Oils," *J. Pet. Tech.* (Nov. 1966) 1487-1490; *Trans.*, AIME, **237**.
13. Stone, H.L.: "Estimation of Three-Phase Relative Permeability and Residual Oil Data," *J. Cdn. Pet. Tech.* (Oct./Dec. 1973) 53-61.
14. Todd, M.R., O'Dell, P.M., and Hirasaki, G.J.: "Methods for Increased Accuracy in Numerical Reservoir Simulators," *Soc. Pet. Eng. J.* (Dec. 1972) 515-530; *Trans.*, AIME, **253**.

APPENDIX

Treatment of Fluid and Rock Properties

Thermal conductivity is treated as a function of gas saturation as

$$\lambda = \lambda_i (1-\alpha_1 S_g) \ , \ldots\ldots\ldots\ldots\ldots\ldots (A\text{-}1)$$

where α_1 should be in the range of 0 to 0.8 and λ_i is a thermal conductivity read as input data. Formation absolute permeability is dependent on solid-phase ($J = 4$) saturation as

$$k = k_i(1+\alpha_2 S_4)\text{md} \ , \ldots\ldots\ldots\ldots\ldots\ldots (A\text{-}2)$$

where α_2 must be zero or negative and k_i is permeability read as input data. Porosity is calculated as $\phi_i[1 + c_r(p - p_i)]$.

Reservoir-rock heat capacity is calculated as

$$M_f = C_{PR}[1 + C_{PRT}\cdot(T-T_i)] \ . \ldots\ldots\ldots (A\text{-}3)$$

The specific volume of a liquid phase is calculated by Amagat's law of partial volumes:

$$v_J = \sum_{I=1}^{N_C} x_{IJ} v_{IJ} \text{ cu ft/mol of phase } J \ . \ldots\ldots\ldots\ldots\ldots\ldots\ldots (A\text{-}4)$$

The partial volume of component I in phase J is

$$v_{IJ} = v^o_{IJ}\big[1+\beta_I(T-T_i)\big]\big[1-c_I(p-p_i)\big], \ldots\ldots\ldots\ldots\ldots\ldots\ldots (A\text{-}5)$$

where v^o_{IJ}, component thermal expansion coefficient β_I, and component compressibility c_I, are read as input data. Liquid-phase density ρ_J is then $1/v_J$. Liquid-water partial volume is calculated as a function of temperature pressure from a read-in table.

Gas-phase density is calculated as

$$\rho_3 = \frac{p}{zRT} \ \frac{\text{mol}}{\text{cu ft}} \ , \ldots\ldots\ldots\ldots\ldots (A\text{-}6)$$

where $R = 10.73$ (here only), and the supercompressibility factor z is calculated from the Redlich-Kwong equation of state.[8]

The specific weight of phase J is

$$\gamma_J = \rho_J M_J/144 \text{ psi/ft} \ , \ldots\ldots\ldots\ldots\ldots (A\text{-}7)$$

where molecular weight is

$$M_J = \sum_{I=1}^{N_C} x_{IJ} M_I \ldots\ldots\ldots\ldots\ldots\ldots (A\text{-}8)$$

The ideal gas-state heat capacity of each component is calculated as

$$C^o_{\text{PI}} = CP1(I) + CP2(I)\,T + CP3(I)\,T^2 \ . \ . (A\text{-}9)$$

The "partial" enthalpy of Component 1 (water) as liquid or vapor is calculated as a function of temperature and pressure from a read-in steam table. The ideal gas-state partial enthalpy of every other component $I (I \neq 1)$ is

$$H^o_I(T) = \int_{T_i}^{T} C^o_{PI} dT \ldots\ldots\ldots\ldots\ldots\ldots (A\text{-}10)$$

Gas-phase enthalpy is calculated as

$$H_3 = \sum_{I=1}^{N_C} x_{13} H^o_I + (H - H^o) \ , \ldots\ldots\ldots (A\text{-}11)$$

where the pressure correction $(H - H^o)$ is calculated using the Redlich-Kwong equation of state.

The partial enthalpy of component I in liquid phase J is

$$H_{IJ} = H^o_I - L_{vIJ}(1-T_{rI})^{0.38}, \ldots\ldots\ldots (A\text{-}12)$$

where L_{vIJ} can be obtained from the two equations (Ref. 10, Page 208)*

$$L_{vb} = 1.093\, RT_c T_{br} \frac{\ln p_c - 1}{0.93 - T_{br}} \ , \ldots\ldots (A\text{-}13)$$

and

$$H^{SV} - H^{SL} = L_{vb}\left(\frac{1-T_r}{1-T_{br}}\right)^{0.38} . \ldots\ldots (A\text{-}14)$$

The enthalpy of liquid phase J is

$$H_J = \sum_{I=1}^{N_C} x_{IJ} H_{IJ} \ , \ldots\ldots\ldots\ldots\ldots (A\text{-}15)$$

*Critical pressure here is in atmospheres.

with H_{IJ} given by Eq. A-12. Internal energy is taken as equal to enthalpy for solid and liquid phases. Internal energy of the gas phase is

$$U_3 = H_3 - 144p/778\rho_3 \quad \text{(A-16)}$$

The gas-phase viscosity is

$$\mu_3 = \sum_{I=1}^{N_C} x_{I3}\mu_{I3} , \quad \text{(A-17)}$$

where

$$\mu_{I3} = VISO(I,3)T^{NVIS(I,3)} , \quad \text{(A-18)}$$

Liquid-phase viscosity is

$$\mu_J = \prod_{I=1}^{N_C} \mu_{IJ}^{x_{IJ}}, \quad \text{(A-19)}$$

where μ_{IJ} is calculated from the ASTM standard form[12]:

$$\ln[\ln(\mu_{IJ}+\gamma\rho]+a\ln T = b , \quad \text{(A-20)}$$

where γ is about 0.6 and ρ is liquid density in grams per cubic centimeter. We drop the term $\gamma\rho$ and place a minimum value on μ_{IJ}. The values of a and b are specified through input data and can be calculated from known values of component viscosity at two temperatures. Eqs. A-17 through A-19 follow Ref. 2. Liquid water viscosity is obtained as a single-valued function of temperature from a read-in table.

The mole fraction of component I in phase J is

$$x_{IJ} = K_{vIJ}X_I , \quad \text{(A-21)}$$

where K_{vIJ} is an equilibrium K-value and X_I is the mole fraction of component I in component I's master or primary phase, J_I. That is, $K_{vIJ_I} \equiv 1.0$. For $J \neq j_I$,

$$K_{vIJ} = \left[K_{V1}(I,J)+K_{V2}(I,J)/p + K_{V3}(I,J)p\right]e^{-\frac{K_{V4}(I,J)}{T-K_{V5}(I,J)}} , \quad \text{(A-22)}$$

where K_{V1} through K_{V5} are read as input data. The form of Eq. A-22 is that used by Crookston *et al.*[2] For water, K_{V13} is calculated as p_s/p, where p_s is water vapor pressure, a single-valued function of temperature. If T exceeds T_c for water, then p_s is taken equal to water critical pressure.

Relative permeability and capillary pressure data may be calculated analytically or interpolated from read-in tables. Analytical calculation of relative permeabilities is as follows.

$$k_{rw} = k_{rwro}(T)\left[\frac{\hat{S}_w - S_{wir}(T)}{1-S_{orw}(T)-S_{wir}(T)}\right]^{n_w} . \quad \text{(A-23)}$$

$$k_{row} = k_{roiw}(T)\left[\frac{1-S_{orw}(T)-\hat{S}_w}{1-S_{orw}(T)-S_{wir}(T)}\right]^{n_{ow}} . \quad \text{(A-24)}$$

$$k_{rog} = k_{roiw}(T)\left[\frac{1-S_{wir}(T)-S_{org}(T)-\hat{S}_g}{1-S_{wir}(T)-S_{org}(T)}\right]^{n_{og}} . \quad \text{(A-25)}$$

$$k_{rg} = k_{rgro}\left[\frac{\hat{S}_g - S^*_{gr}}{1-S_{wir}-S_{org}-S^*_{gr}}\right]^{n_g} . \quad \text{(A-26)}$$

Stone's second method,[13] in modified form, is used to calculate oil relative permeability as

$$k_{ro} = k_{roiw}(T)\left[\left(\frac{k_{row}}{k_{rocw}(T)}+k_{rw}\right)\cdot\left(\frac{k_{rog}}{k_{roiw}(T)}+k_{rg}\right)-k_{rw}-k_{rg}\right] . \quad \text{(A-27)}$$

Gas relative-permeability hysteresis is handled as follows.

$$S_{grc} = S_{gr}\frac{(\hat{S}_g)_{\max}}{1-S_{wir}-S_{org}} , \quad \text{(A-28)}$$

where S_{grc} is current residual gas saturation, $(\hat{S}_g)_{\max}$ is historical maximum gas saturation in the grid block from start of the run, and S_{wir} and S_{org} are read in (nontemperature-dependent values). S_{gr} is read-in residual gas saturation. S_{grc}, after calculation from Eq. 6, is changed to satisfy $S_{gc} \leq S_{grc} \leq S_{gr}$, where S_{gc} is read-in critical gas saturation and $S_{gr} \geq S_{gc}$. Current effective residual gas saturation (S^*_{gr}) for use in Eq. A-26 is calculated as

$$S^*_{gr} = \omega S_{grc} + (1-\omega)S_{gc} , \quad \text{(A-29)}$$

where

$$\omega = \frac{(\hat{S}_g)_{\max}-\hat{S}_g}{(\hat{S}_g)_{\max}-S_{grc}} . \quad \text{(A-30)}$$

As long as S_g is increasing, always $\geq (S_g)_{\max}$, these equations give $S^*_{gr} = S_{gc}$, and k_{rg} from Eq. A-26 will follow the "original" k_{rg} vs. S_g curve. Then, as S_g decreases toward zero, k_{rg} will approach zero at S_{grc}.

This hysteresis is generally not important and has an effect (not a large one, from our experience) only in cyclic steam stimulation runs.

Gas-phase relative permeability is treated with no temperature dependence.

The temperature-dependent quantities $S_{wir}(T)$, $k_{rwro}(T)$, etc., all are treated as

$$X = X^o + \alpha(T-T_i) , \quad \text{(A-31)}$$

where X^o and the temperature derivatives (α) are read in as data.

The normalized saturations in the above equations are

$$\hat{S}_w = \frac{S_w}{1-S_4} ,$$

$$\hat{S}_o = \frac{S_o}{1-S_4} ,$$

and

$$\hat{S}_g = \frac{S_g}{1-S_4} .$$

Analytical expressions for capillary pressures are

$$P_{cwo}(\text{psi}) = \left[PCC(1) + PCC(2) \times (1-\hat{S}_w)\right] + PCC(3) \times (1-\hat{S}_w)^3\Big] \times \left[1 - PCC(4) \times (T - T_i)\right], \ldots \text{(A-32)}$$

and

$$P_{cgo}(\text{psi}) = \left[PCC(5) + PCC(6) \times \hat{S}_g + PCC(7) \times \hat{S}_g^3\right] \times \left[1 - PCC(8) \times (T - T_i)\right]. \ldots\ldots\ldots\ldots \text{(A-33)}$$

$PCC(1)$ through $PCC(8)$ are input data. The temperature dependence uses the assumption that interfacial tension is a linear function of temperature.

SI Metric Conversion Factors

°API		141.5/(131.5 + °API)	=	g/m^3
atm	×	1.013 250* E+02	=	kPa
bbl	×	1.589 873 E−01	=	m^3
Btu	×	1.055 056 E+00	=	kJ
cp	×	1.0* E−03	=	Pa·s
cu ft	×	2.831 685 E−02	=	m^3
°F		(°F − 32)/1.8 + 273.18	=	K
ft	×	3.048* E−01	=	m
lbm	×	4.535 924 E−01	=	kg
lbm mol	×	4,535 924 E−01	=	kmol
psi,psia	×	6.894 757 E+00	=	kPa
scf	×	2.863 640 E−02	=	std m^3
sq ft	×	9.290 304* E−02	=	m^2

*Conversion factor is exact.

SPEJ

Original manuscript received in Society of Petroleum Engineers office Sept. 23, 1979. Paper accepted for publication April 21, 1980. Revised manuscript received Aug. 18, 1980. Paper (SPE 8394) first presented at the SPE 54th Annual Technical Conference and Exhibition, held in Las Vegas, Sept. 23-26, 1979.